UNITED NATIONS EDUCATIONAL, SCIENTIFIC AND CULTURAL ORGANIZATION
INTERNATIONAL ATOMIC ENERGY AGENCY
INTERNATIONAL CENTRE FOR THEORETICAL PHYSICS
I.C.T.P., P.O. BOX 586, 34100 TRIESTE, ITALY, CABLE: CENTRATOM TRIESTE

H4.SMR/916 - 13

SEVENTH COLLEGE ON BIOPHYSICS:

Structure and Function of Biopolymers: Experimental and Theoretical Techniques.

4 - 29 March 1996

Neutron Scattering in Biology

A. DERIU
Dipartimento di Fisica
Universita' di Parma
Istituto Nazionale di Fisica della Materia
Parma, ITALY

NEUTRON SCATTERING IN BIOLOGY

Antonio Deriu

Dipartimento di Fisica, Università di Parma,

and Istituto Nazionale di Fisica della Materia

Viale delle Scienze, I-43100 Parma, Italy

I. INTRODUCTION

Biological materials at a molecular level are heterogeneous systems: they are made up from a heteropolymeric skeleton (polynucleotides, polypeptides, polysaccharides) or from complex multilayered sheets (lipid membranes) in interaction with an aqueous buffer. Water plays a major role in stabilizing the large scale arrangement (ternary and quaternary structures) of biomolecular assemblies and controls the activation of most biological processes. It is precisely this 'composite' nature combining the high degree of mechanical stability of the solid biopolymer scaffolding with the liquid-like behaviour of the buffer, which accounts for the enormous structural and functional diversity of macromolecules in living systems.

Not only structure but also motion is of great importance at the molecular level of biology. The marked temperature dependence of the activity of biomolecules reflects their thermal mobility. A characterization at a microscopic scale of processes and interactions responsible for molecular flexibility and dynamics is a necessary starting point for a deeper understanding of the mechanisms which control the highly specific functions of most biological materials.

Diffraction and spectroscopic studies aiming at understanding the macroscopic behaviour of biomolecular systems in terms of molecular parameters focus on altered hydrogen-bonding patterns, on changes in the dynamic variables through translational or rotational correlation functions. Thermal and cold neutrons are excellent probes for for such studies on the 'dynamic structuring' of biomolecular assemblies due to the fact that structural information (from elastic scattering), and dynamic information (from inelastic scattering) can be

obtained simultaneously over a quite large space-time domain.

The use of neutron diffraction and scattering in studying the structure and dynamics of soft-matter systems is well established nowadays. The main limitation of these techniques is connected with the relatively low intensity of even large-scale sources. A high-flux reactor ($\sim$ 60 MW) produces about $2 \cdot 10^{18}\ ns^{-1}$ corresponding to a 1/3 W optical lamp. Moreover the density of thermal neutrons produced is of the order of $10^{17}\ n\ \mathrm{m}^3$; to get the same density of air, one has to pump to a pretty good vacuum ($\sim 10^{-7}$ mbar). This means that neutrons are really scarce, and they should be used 'intelligently' i.e they should come into play only when other techniques (X-rays, optical spectroscopies, and other nuclear spectroscopies) can not do the job.

Despite these limitations, neutrons have some intrinsic advantages and peculiarities which make them in many cases unique and fully justify their use as soft-matter probes. Neutrons interact with atoms mostly through the so-called 'strong interaction' with nuclei, and through the magnetic interaction between its magnetic moment and the atomic magnetic moments. The first interaction extends over the size od a nuclear radius, typically 10^{-12} cm or less. This size is much smaller than the wavelength of thermal neutrons (typically $\sim 10^{-8}$ cm). the interaction can therefore be practically considered as pointlike, and when averaged over atomic scale distances, quite weak; indeed the mean free path of a neutron in a solid is of the of centimeters. Moreover the interaction, being of nuclear origin is completely independent of the chemical environment, and has no special trend along the periodic table. This fact makes it possible to distinguish contributions from even contiguous elements in a diffraction profile.

II. BASIC THEORY

We assume to describe the scattering of a neutron by a single nucleus in terms of the interaction between an incoming wave of wavelength $\lambda_N = h/p$ (de Broglie wavelength) and an appropriate matter density function $\rho_N(\boldsymbol{r})$. Then by summing over contributions from

all different volume elements with the appropriate phase differences we have:

$$\psi = A \int exp(i\boldsymbol{K}_i \cdot \boldsymbol{r})\, exp(-i\boldsymbol{K}_f \cdot \boldsymbol{R}_\circ)\, \rho(\boldsymbol{r} - \boldsymbol{R}_\circ) d\boldsymbol{r} \tag{1}$$

There $\boldsymbol{R}_\circ$ is the position of the nucleus, A is a constant which depends on the nature of the neutron-nucleus interaction, $\boldsymbol{K}_i$ and $\boldsymbol{K}_f$ are the incoming and outgoing wavevectors of the neutron, and the integration is carried out over the volume where $\rho_N(\boldsymbol{r})$ is different from zero. Taking into account the typical size of nuclei which is about 10^3 smaller than λ_N, we can conclude that $(K\ r) \leq 10^{-3}$ and therefore eq. (1) can be approximated to:

$$\psi = const \cdot exp(-i\,\boldsymbol{Q} \cdot \boldsymbol{R}_\circ) \tag{2}$$

where $\boldsymbol{Q}$ is the momentum transfer $\boldsymbol{Q} = \boldsymbol{K}_f - \boldsymbol{K}_i$. The flux of neutrons scattered into the direction defined by $\boldsymbol{K}_f$ is proportional to $\mid \psi^2 \mid$ and is therefore isotropic and specified by a single constant dependent on the specific nucleus only. When more than one nucleus is present, the total amplitude is obtained by summing over all the nuclei at sites $\boldsymbol{R}_l$:

$$\psi = const \cdot \sum_l exp(i\,\boldsymbol{Q} \cdot \boldsymbol{R}_l) \tag{3}$$

and the flux of scattered neutrons is given by:

$$\phi = B \mid \psi \mid^2 = const \cdot \sum_l \sum_s A_l\, A_s\, exp(i\,\boldsymbol{Q} \cdot (\boldsymbol{R}_l - \boldsymbol{R}_s)) \tag{4}$$

in terms of appropriate constants A_l and A_s describing the scattering from single nuclei. It is usual to introduce a quantity called the scattering cross section, which depends only on the scattering process and is independent of the incoming-beam intensity. This is defined as the ratio of the flux $d\phi$ (number of neutrons per unit time) of neutrons scattered within solid angle $d\Omega$ and having energy $E_f = E_i \pm \hbar\omega$ to the incoming-beam intensity $I_\circ$ (number of neutrons per unit area and time):

$$d\phi = \frac{d^2\sigma}{d\Omega d\omega}\, I_\circ\, d\Omega\, d\omega \tag{5}$$

there $\hbar\omega$ represents the neutron energy transfer to the sample and is given by:

$$\hbar\omega = E_i - E_f = \frac{\hbar^2}{2m_N}(K_i^2 - K_f^2) \tag{6}$$

If we consider purely elastic scattering, then $E_i = E_f$ and we have:

$$d\phi = \frac{d\sigma}{d\Omega} I_\circ \, d\Omega \tag{7}$$

and according to eq. (4) the scattering cross section from a single nucleus can be expressed in terms of a single constant b called scattering amplitude:

$$\frac{d\sigma}{d\Omega} = const. = \mid b^2 \mid \tag{8}$$

The extension to the case of many nuclei can be performed by analogy to eq. (4):

$$\frac{d\sigma}{d\Omega} = \sum_l \sum_s b_l \, b_s \, exp(i\,\boldsymbol{Q}\cdot(\boldsymbol{R}_l - \boldsymbol{R}_s)) \tag{9}$$

In the above equation it is useful to single out the effect of the fluctuations of the scattering amplitudes. These are due to the fact that the amplitudes b_l depend on the specific scattering nucleus and on its nuclear spin. In a real sample therefore fluctuations arise due to both isotopic distribution and to nuclear spin disorder. We can therefore split b_l into its average value and its fluctuation as:

$$b_l = \bar{b} + \Delta b_l \tag{10}$$

for the fluctuations, assuming a random occupancy of sites l and s, we have the following average values: $\overline{\Delta b} = 0$ and $\overline{\Delta b_l \Delta b_s} = \overline{\Delta b_l^2}\,\delta_{ls}$.

We can now substitute eq. (10) into eq. (9) to get

$$\frac{d\sigma}{d\Omega} = \sum_l \sum_s \mid \bar{b} \mid^2 exp(i\,\boldsymbol{Q}\cdot(\boldsymbol{R}_l - \boldsymbol{R}_s)) + N\overline{\Delta b_l^2} \tag{11}$$

The first term (usually referred to as 'coherent scattering') depends on the nuclear positions and gives rise to diffraction effects through the interference of different waves. The second term ('incoherent scattering') is constant with respect to Q, and depends only the nature of the sample. It must be emphasized that the notion of coherence and incoherence

do not have the same significance for the X-ray and neutron communities. For the neutron users, coherence is related mostly to nuclear spin coherence, and neutron scattering always displays two components: a 'coherent' one and an 'incoherent'. For X-ray users coherent refers to the existence of correlations between the deviations from a perfect three-dimensional structure. The extent of the correlations can vary from intramolecular distances up to an entire crystal. Therefore only 'coherent' and 'correlated' neutron scattering corresponds to the 'coherence' of the X-ray community.

III. ELASTIC SCATTERING

In the case of ordered systems (crystals) the nuclear positions belong to a three-dimensional translation group, therefore each position vector can be expressed as the sum of the vector position of a unit cell and a vector position within the unit cell:

$$\boldsymbol{R}_{lj} = \boldsymbol{R}_l + \boldsymbol{r}_j \tag{12}$$

where l runs over the N cells in the crystal and j over the nuclei present in the unit cell. Then by substituting eq. (10) and eq. (12) into eq. (11), and thanks to the fact that $\overline{\Delta b_l \Delta b_j} = 0$, we can split the cross-section into two contributions. We thus obtain:

$$\begin{aligned} \frac{d\sigma}{d\Omega} = & \quad \mid \textstyle\sum_j \bar{b}_j \, exp(i\,\boldsymbol{Q}\cdot\boldsymbol{r}_j) \sum_l exp(i\,\boldsymbol{Q}\cdot\boldsymbol{R}_l) \mid^2 + \\ & + N \textstyle\sum_j \sum_k \sum_l \overline{\Delta b_{lj} \Delta b_{lk}} \, exp(i\,\boldsymbol{Q}\cdot(\boldsymbol{r}_j - \boldsymbol{r}_k)) \, exp(i\,\boldsymbol{Q}\cdot\boldsymbol{R}_l) \end{aligned} \tag{13}$$

Because of the lattice periodicity $\sum_l exp(i\,\boldsymbol{Q}\cdot\boldsymbol{R}_l)$ is equal to N if $\boldsymbol{Q}$ is a reciprocal-lattice vector, and is zero otherwise, namely:

$$\sum_l exp(i\,\boldsymbol{Q}\cdot\boldsymbol{R}_l) = N \sum_{\boldsymbol{G}} \delta_{\boldsymbol{Q}\boldsymbol{G}} = \frac{(2\pi)^2}{\Omega_o} \sum_{\boldsymbol{G}} \delta(\boldsymbol{Q} - \boldsymbol{G}) \tag{14}$$

This is a way of formulating the well known Bragg law in terms of the reciprocal-lattice vectors which are defined by the following relation:

$$\boldsymbol{G} \cdot \boldsymbol{R}_l = 2n\pi \tag{15}$$

and are given by $\boldsymbol{G} = h\boldsymbol{a}_1 + k\boldsymbol{a}_2 + l\boldsymbol{a}_3$, where the $\boldsymbol{a}_i$ define the unitary vector in the reciprocal lattice.

We can therefore conclude that the elastic cross-section (eq. (13)) results as the sum of two terms. The first (Bragg scattering) is non-zero only for selected values of the momentum transfer $\boldsymbol{Q}$. The second (incoherent scattering) is generally a smoothly varying function, and it can provide information on local environments in partially disordered systems.

If one wants to study disordered systems the starting point is still eq. (11); by separating coherent and incoherent contribution in a way analogous to that done previously one obtains for the scattering cross-section:

$$\frac{d\sigma}{d\Omega} = \sum_{\alpha\beta} b_\alpha \, b_\beta \, S_{\alpha\beta}(\boldsymbol{Q}) + N \, \overline{\Delta b_l^2} \tag{16}$$

The $S_{\alpha\beta}(\boldsymbol{Q})$ function is called the partial structure factor. Its Fourier transform $G_{\alpha\beta}(\boldsymbol{r})$ provides the distribution of the relative distances between atoms α and β, and it is given by:

$$G_{\alpha\beta} = \frac{1}{(2\pi)^3} \int exp(i\,\boldsymbol{Q} \cdot \boldsymbol{r}) \, S_{\alpha\beta}(\boldsymbol{Q}) \, d\boldsymbol{Q} = \sum_{ls} \overline{\delta(\boldsymbol{r} - \boldsymbol{R}_l + \boldsymbol{R}_s)_{l_\alpha s_\beta}} \tag{17}$$

IV. INELASTIC SCATTERING

We have so far assumed that nuclei are fixed in specific positions in space, this is not true even at low temperatures. and typical vibrational frequencies ($\leq 10^{13}$) correspond to energies up to ~ 50 meV, which are comparable to the energies of thermal neutrons (a neutron with an energy of 50 meV has a wavelength $\lambda = 0.78$ Å). In order to obtain the cross-section as defined in eq. (5) we have to generalize eq. (1), and consider a time-dependent wave amplitude:

$$\psi = \int exp(i\boldsymbol{K}_i \cdot \boldsymbol{r}) \, exp(-i\boldsymbol{K}_f \cdot \boldsymbol{r}) \, \rho_N(\boldsymbol{r} - \boldsymbol{R}_o(t)) \, d\boldsymbol{r} \tag{18}$$

The energy dependent flux can then be evaluated in terms of the Fourier transform of the squared wave amplitude:

$$\phi(\omega) \propto \int exp(-i\omega t)\,\langle exp(i\,\boldsymbol{Q}\cdot\boldsymbol{R}_{\circ}(0))\,exp(-i\,\boldsymbol{Q}\cdot\boldsymbol{R}_{\circ}(t))\rangle dt \tag{19}$$

where the average $\langle\cdots\rangle$ is taken over all possible vibrations. Then the generalization of eq. (19) to the case of many nuclei can be obtained, and the double differential cross-section eq. (5) can be written as:

$$\frac{d^2\sigma}{d\Omega d\omega} = \frac{1}{2\pi}\sum_{lk} b_l b_k \int exp(-i\omega t)\,\langle exp(i\,\boldsymbol{Q}\cdot\boldsymbol{R}_l(0))\,exp(i\,\boldsymbol{Q}\cdot\boldsymbol{R}_k(t))\rangle dt \tag{20}$$

In the following, starting from the above general equation, we will consider two simple cases; the elastic Bragg scattering in the case of moving nuclei, and the inelastic scattering from a high-frequency sound wave (phonon).

A. The Debye-Waller Factor

Let us now derive the purely elastic scattering from eq. (20). In such a case the nuclear positions can be expressed as a sum of a time- independent equilibrium position ($\boldsymbol{R}(0)$), and a (small) time-dependent displacement ($\boldsymbol{u}(t)$) from equilibrium

$$\boldsymbol{R}_l(t) = \boldsymbol{R}_l(0) + \boldsymbol{u}_l(t) \tag{21}$$

The displacements become uncorrelated when t becomes large, and therefore in the limit $t \to \infty$ we can substitute $\langle\cdots\rangle$ with $\langle\cdots\rangle\,\langle\cdots\rangle$ in eq. (20). Then each average can be evaluated easily assuming a Gaussian distribution of displacements to give:

$$\langle exp(i\,\boldsymbol{Q}\cdot(\boldsymbol{R}_l(0) + \boldsymbol{u}_l(t)))\rangle = exp(i\,\boldsymbol{Q}\cdot\boldsymbol{R}_l(0))\;exp(-W_l) \tag{22}$$

where the Debye-waller factor $exp(-W_i)$ is given by:

$$exp(-W_l) = \prod_{\alpha=1}^{3} exp(-Q_\alpha^2\,\langle u_{l\alpha}^2\rangle) \tag{23}$$

Using this result eq. (13) can be rewritten showing explicitly the Debye-waller factors:

$$\frac{d\sigma}{d\Omega} = \mid \sum_j \bar{b}_j \, exp(-W_j) \, exp(i\,\boldsymbol{Q}\cdot\boldsymbol{r}_j) \, \sum_{\boldsymbol{G}} \delta_{\boldsymbol{Q}\boldsymbol{G}} \mid^2 +$$

$$+ N \sum_j \sum_k \sum_l \overline{\Delta b_{lj} \Delta b_{lk}} \, exp(-W_j - W_k) \, exp(i\,\boldsymbol{Q}\cdot(\boldsymbol{r}_j - \boldsymbol{r}_k)) \, exp(i\,\boldsymbol{Q}\cdot\boldsymbol{R}_l) \quad (24)$$

The Debye-Waller is a decreasing function of momentum transfer Q, and therefore it produces only a decrease of the intensity of the elastic-scattering contribution at high momentum transfer.

B. Inelastic Phonon Scattering

If we consider an ideal crystal we can describe harmonic vibrations as sinusoidal deviations from the equilibrium positions:

$$\boldsymbol{u}_l(t) = \boldsymbol{e}_{\boldsymbol{q}j} \; exp(i\boldsymbol{q}\cdot\boldsymbol{R}_l(0) \, exp(i\omega_{\boldsymbol{q}j}t) \quad (25)$$

where $\boldsymbol{q}$ and $\omega_{\boldsymbol{q}j}/2\pi$ are the wave vector and frequency respectively of the sinusoidal wave, $\boldsymbol{e}_{\boldsymbol{q}j}$ is its the polarization vector, and j the branch index. Then we can rewrite eq. (20) as:

$$\left(\frac{d^2\sigma}{d\Omega d\omega}\right)_{in} = \frac{1}{2\pi} \sum_{lk} b_l b_k \, exp(i\,\boldsymbol{Q}\cdot(\boldsymbol{R}_l(0) - \boldsymbol{R}_k(0)) \cdot$$

$$\cdot \int exp(-i\omega t) \, exp(i\,\boldsymbol{Q}\cdot\langle \boldsymbol{u}_l(0)) \, exp(i\,\boldsymbol{Q}\cdot\boldsymbol{u}_k(t))\rangle \, dt \quad (26)$$

We can now substitute eq. (25) into the previous one to obtain:

$$\left(\frac{d^2\sigma}{d\Omega d\omega}\right)_{in} = N^2 b^2 \mid \boldsymbol{Q}\cdot\boldsymbol{e}_{\boldsymbol{q}j} \mid^2 \sum_{\boldsymbol{G}} \delta_{\boldsymbol{Q}-\boldsymbol{G},\boldsymbol{q}} \delta(\omega - \omega_{\boldsymbol{q}j}) \quad (27)$$

This is a highly simplified expression not only because a single scattering amplitude b is assumed, but mainly because we have tacitly assumed that only one wave is present, however it contains the most relevant physical features. The correct complete expression of the inelastic phonon cross-section is:

$$\left(\frac{d^2\sigma}{d\Omega d\omega}\right)_{in} = N^2 b^2 \frac{K_f}{K_i} \frac{1}{2m} \sum_{\boldsymbol{G}} \mid \boldsymbol{Q}\cdot\boldsymbol{e}_{\boldsymbol{q}j} \mid^2 \frac{1}{\omega_{\boldsymbol{q}j}} \cdot$$

$$\{n(\omega_{\boldsymbol{q}j}) \, \delta(\omega + \omega_{\boldsymbol{q}j}) \, \delta_{\boldsymbol{Q}+\boldsymbol{q},\boldsymbol{G}} + (n(\omega_{\boldsymbol{q}j}) + 1) \, \delta(\omega - \omega_{\boldsymbol{q}j}) \, \delta_{\boldsymbol{Q}+\boldsymbol{q},\boldsymbol{G}}\} \quad (28)$$

where $n(\omega)$ indicates the Bose population factor: $n(\omega) = \{exp(\hbar\omega/K_B T) - 1\}^{-1}$.

V. NEUTRON CRYSTALLOGRAPHY OF BIOLOGICAL MOLECULES

In the past few years the number of biomolecular structures determined by single-crystal diffraction techniques has increased enormously. This progress has been due to improvements in the X-ray sources and instrumentation (synchrotron radiation plays a relevant role in this context nowadays), in the structure solution techniques employing more and more powerful computers, and in the crystallization procedures and biomolecular engineering techniques.

The applications of neutron diffraction techniques in biology are highly complementary to X-rays and are mostly used to elucidate particular aspects of the biomolecular structures. Once the overall features are known, neutrons are used to study what can not be seen by X-rays.

An important advantage of neutrons is the high scattering power of hydrogen and deuterium. Their scattering lengths are comparable or greater to that of heavier atoms as oxygen, carbon, and nitrogen, thus the signals from deuterium and carbon are nearly equal for neutrons, while deuterium or is only 3 % of the signal from carbon in the X-ray case. In addition the neutron scattering lengths for hydrogen and deuterium are very different. In cases where atomic resolution can not be reached, for instance in the case of partially disordered systems, neutrons can single out specific features. The easiest case in which the H/D exchange can be performed is that of water. This is currently used in the study of biological materials which always contain a considerable amount of water. The procedure is called 'contrast variation'. The solvent is made up by a suitable mixture of H_2O and D_2O in varying ratios. The scattering density is -0.06 fm/Å^3 for H_2O, and 0.63 fm/Å^3 for D_2O. The value for proteins is typically around 0.25 fm/Å^3, while for DNA or RNA this number is about 0.42 fm/Å^3. By a suitable choice of the H/D mixture the signal from either component with respect to that of the solvent can therefore be reduced or enhanced.

In a diffraction experiment we measure scattering intensities $I_{\boldsymbol{h}}$ reflected off the different sets of Bragg planes $\boldsymbol{h} = (h, k, l)$ of the crystal. $I_{\boldsymbol{h}}$ is related to the so-called structure factor $F_{\boldsymbol{h}}$ by:

$$I_{\boldsymbol{h}} = (experimental\ constants) \times \mid F_{\boldsymbol{h}} \mid^2 \tag{29}$$

and

$$F_{\boldsymbol{h}} = \int\int\int \rho(x,y,z)\, exp(-2\pi i\,(hx + ky + lz))\; dV \tag{30}$$

where$\rho(x,y,z)$ is the scattering density at the point (x,y,z).

For a distribution ρ made up of atoms, $F_{\boldsymbol{h}}$ can be expressed as a sum over the atoms:

$$F_{\boldsymbol{h}} = \sum_j b_j\, exp(-2\pi i\,(hx_j + ky_j + lz_j))\, exp(-W_j) \tag{31}$$

The two above expressions are both used. The density approach is more convenient when most of the structure is known and one looks for the effect of small and usually local modifications of the starting structure. In this case one deals with the difference:

$$\Delta\rho(x,y,z) = \rho(x,y,z)_{new} - \rho(x,y,z)_{known} \tag{32}$$

and the two densities are obtained from the experimental intensities and eq. (31).

In the 'atomic model' approach the exact atomic positions and mean square displacements are investigated. The calculation is usually done by some kind of non-linear least-squares method, minimizing a quantity of the type:

$$\sum_{\boldsymbol{h}} w_{\boldsymbol{h}} (\mid F_{\boldsymbol{h}}^{obs} \mid - \mid F_{\boldsymbol{h}}^{calc} \mid)^2 \tag{33}$$

A. High Resolution Studies

The first neutron diffraction study of myoglobin dates back to 1969. It showed that it was possible to locate ordered hydrogen and deuterium atoms from density maps at a 2.0 Å resolution. Various important studies of this kind then followed mostly aiming at locating specific hydrogen atoms that are key parts of an enzymatic process.

An example of this kind is the identification of the catalytic base in the active site of trypsin. This is an enzyme which hydrolyses the peptide bond on the carboxyl side of lysine

and arginine, and the catalytic site holds three invariant residues: a histidine, an aspartic acid, and a serine. Two models were proposed for the intermediary state, which differed only in the protonation state of histidine. The atoms of interest were determined from different kinds of scattering density and difference maps, and it was possible to select one of the two proposed models as the most likely intermediary in the reaction.

Water itself is obviously a main target for study. Oxygens from waters of hydration can be easily seen with X-rays, but this information is not usually sufficient to identify a hydrogen bonding network. A clear example is that of vitamin B_{12}. This 'small' molecule (209 atoms) in crystal form binds about 17 waters per molecule. Starting from the X-ray density maps which gave the oxygen locations, the neutron high resolution data provided a full description of the scattering densities from hydrogens and provided also some indication that the 'disorder' observed in the hydrogen positions is dynamic in origin.

Interesting combined X-ray and neutron diffraction studies have also been performed on fibrous biopolymers. In many biological structures such as muscle and connective tissue the fibrous state is is functionally important and fibre diffraction provides the most powerful technique to investigate the molecular and supramolecular structure. The most popular biopolymer which can be prepared in fibrous form is DNA; in this case diffraction studies provide information also on the molecular polymorphism (highly cooperative structural transitions between different conformational DNA scaffoldings). In this field X-ray fibre diffraction with sinchrotron radiation has provided a quite extensive information on molecular conformations and transitions. neutron diffraction on the other hand has greatly contributed in locating order water molecules associated to the DNA double helices, this is a very valuable information since it is known that water plays a key role in stabilizing the various DNA conformations and in mediating structural transitions between them. Difference density maps obtained from fully H_2O and fully D_2O exchanged samples have identified the existence of an extensive order water network in the minor and major grooves of the DNA double helices.

Neutrons can also be used to follow H/D exchange for periods ranging from days to

years. One example comes from the analysis of trypsin. In this case a protein crystal originally grown in H_2O was soaked for one year in a D_2O buffer, and then re-measured. It was found that 68 % of the exchangeable amide protons in the peptide units was indeed exchanged. It was also observed that the non-exchanged hydrogens were found mainly in the $\beta-$sheet regions, which in this structure form the so called $\beta-$barrels. Information about local dynamics can be also extracted. The H/D pattern in the residues 47-52 of trypsin provides an example of this kind. The bend formed by the residues could be in principle 'opened' in different ways. The data on exchanged and non-exchanged hydrogens in such residues tend to exclude 'zipper' type motions which would 'release' all the hydrogen bonds between the two chains, they rather suggest H/D exchange mechanisms of more local nature.

B. Low Resolution Studies

When a substantial part of a biomolecular assembly is disordered the goal is to get low resolution information (typically at $\sim 8-16$ Å resolution level), and thus provide information on the location of the various components of the macromolecular system. For these studies long wavelength ($8-10$ Å) are best suited. These are available with cold neutrons, but not with X-rays.

As an example of a low resolution study we can mention the case of lipovitellin, a protein of about 352,000 D weight, which binds lipids. The best way to prove that such lipids are located in the middle cavity of the protein scaffolding is to perform a low resolution contrast variation experiment with neutrons. Measurements were performed in different buffers with varying H/D ratios; in this way it was possible to make the protein 'invisible' to neutrons, and to show that there is indeed some density inside the protein. Based on the fact that the match point of lipids differs from that of polypeptides, it was possible to ascribe this density to the lipids which seems to be bound in a bilayer. This configuration is energetically favoured by the hydrofobic nature of the lipid-protein interactions.

VI. SMALL ANGLE NEUTRON SCATTERING

Many macro- and biomolecules can be easily dissolved into suitable solvents giving rise to 'colloidal systems'. On the base of the macromolecule-solvent interactions three main categories can be identified: lyophobic (solvent hating), lyophilic (solvent loving), and association colloids. The latter are formed by aggregates of amphiphilic molecules. A typical example is that of surfactants: in this case the macromolecules have a polar head group at one end and a water insoluble aliphatic chain on the other end. As the concentration of such molecules is raised in an aqueous solution, globular micellar aggregates can form, and by increasing concentration these can change into cylindrical or disklike micelles. In the case of suspension of large biomolecules like proteins, the colloidal particles are just the biomolecules themselves: proteins in water tend to form lyophilic colloids. An other very interesting family is that of biopolymer gels. These are formed by long polymer chains which give rise to a loose 3D random network either by chemical inter-chain cross-links (chemical gels), or by 'physical' interactions which produce an 'entanglement network'. In the latter case the gelation process is usually thermoreversible since the cross-links themselves are of small but finite energy, and/or finite lifetime. Such polymer networks are able to 'trap' large solvent volumes, and the dynamic properties of these solvent molecules are significantly different from those of 'bulk' solvent, even at very low polymer concentration.

We will here focus on the static properties, and we will describe the main features of small angle neutron scattering (SANS) techniques; these will be compared with similar techniques which make use of X-ray scattering (SAXS), and static light scattering (SLS). These topics have been object of recent reviews. The general results we will derive apply to all the three techniques.

Small-angle scattering techniques (SANS, SAXS, and SLS) allow us to obtain structural information about inhomogeneities in materials. Comprehensive references of small angle scattering techniques are the classical books by Glatter and Kratky, and, earlier by Guinier and Fournet. SAXS is sensitive to inhomogeneities of the electron density, neutrons reveal

the variation of the so-called scattering length density, while light is sensitive to variations of the refractive index n. As already pointed out in Sec. I and II, a fundamental theorem of the wave scattering theory relates the real-space density distribution of a scattering object to the $Q-$space scattered intensity distribution by a Fourier transform.

In small angle scattering experiments one measures predominantly the elastic scattering from an isotropic medium, therefore: $\mid \boldsymbol{K}_i \mid = \mid \boldsymbol{K}_f \mid = 2\pi/\lambda$; consequently the magnitude of the momentum transfer vector $\boldsymbol{Q}$ is:

$$Q = (4\pi/\lambda)\, n\, sin\theta \tag{34}$$

where 2θ is the scattering angle. The refractive index n for light is $\simeq 1.33$ in the case of water, which is the most used solvent. For neutrons and X-rays n is very close to unity.

From the above mentioned Fourier theorem it follows that the characteristic size of an object in real-space R is reciprocally related to the characteristic width of the scattering intensity distribution in Q-space ($Q = 2\pi/R$). Thus neutrons and X-rays may be used to probe 'particles' in the 10-1000 Å range, while SLS ($\lambda = 4000 - 8000$ Å) is needed in the 1000 Å to μm range. An other important element to consider is the nature of the interaction between the radiation and the particles in the medium.

- *light scattering* - The probe is a photon ($E \sim 10$ eV, $\lambda \sim 5000$ Å). The interaction is with the polarizability α of the scatterer, and a scattering length can be defined as:

$$b(\theta, \lambda, \alpha) = f(\theta)\, \alpha\, k_o^2 \tag{35}$$

here $k_o = 2\pi/\lambda$. The factor $f(\theta)$ originates from the polarization of the incident and scattered beam. The polarizability α can be related to the refractive index n and to the concentration of scatterers N/V. Assuming isotropy the following relation holds:

$$\alpha = \frac{3}{4\pi}\frac{V}{N}\frac{n^2 - 1}{n^2 + 2} \tag{36}$$

this always gives $b > 0$.

- *X-ray scattering* - The probe is now a more energetic photon ($E \sim 10^4$ eV, $1 < \lambda < 5$ Å). The scattering length in this case has a very simple dependence upon the number of electrons z of the scattering atom:

$$b = b_o\, z; \qquad\qquad b_o = -0.282\, 10^{-12}\text{cm} \tag{37}$$

- *Neutron scattering* - The neutrons used in SANS have an energy of about 10^{-3} eV ($1 < \lambda < 20$ Å). As noticed in Sec. II value of b is dependent on the nature of the nuclei, and is sensitive to the state of the nuclear spin. The b values are experimentally determined and tabulated. The best known example is that of hydrogen whose b value ($-0.374\, 10^{-12}$ cm) is very different from that its first isotope, deuterium ($b = +0.667\, 10^{12}$ cm). The isotopes and the spin values are randomly distributed among the atom sites. Due to this disorder we have to deal both with a coherent contribution, and with a Q-independent incoherent scattering, which gives a background-like level. This has to be subtracted from the diffraction pattern.

Although SANS is in many respect similar to SAXS and SLS, it has some peculiarities which can be of great advantage in the study of complex biomolecular solutions:

(*i*) The measure of the absolute scattering cross section is relatively easy. The contribution from the container cell and from impurities in the solvent are generally not a problem due to the relatively short (with respect to SLS) wavelength used ($5 - 20$ Å). Multiple scattering is usually negligible since it is relatively easy to keep the transmission of the sample above ~ 80 %.

(*ii*) The coherent scattering length density of the solvent can be continuously varied by simply changing the D_2O/H_2O. Contrast matching techniques allow one to 'eliminate' the scattering contribution from a particular species in a multicomponent system.

(*iii*) The possibility of selectively deuterating specific parts of or functional groups in a macromolecule makes it possible to enhance the spatial resolution of an experiment.

A modern SANS instrument uses neutrons from a cold source. The wavelength of incoming neutrons is defined by an helical slot selector ($\Delta\lambda/\lambda \simeq 10$ %). Neutrons that are scattered at an angle 2θ are detected by a two-dimensional multidetector (a typical sys-

tem has 64×64 cells, each 10 x 10 mm^2). Its distance from the sample can be varied by moving the detector system inside a vacuum tube. The scattering vector Q, for a given sample-to-detector distance L is then given by:

$$Q = \frac{2\pi}{\lambda} tan\theta \simeq \frac{2\pi}{\lambda}\frac{d}{L} \tag{38}$$

The instrument D11 at the ILL (Grenoble) has a maximum $L = 35$ m. At such distance, using 20 Å neutrons, it is possible to reach a minimum $Q \leq 0.001$ Å^{-1}.

In evaluating the scattering cross section, the so-called static approximation is used, and inelasticity corrections are in most cases neglected because the masses of the molecules are far greater than the neutron mass. The scattering cross section is then given by:

$$\frac{d\sigma}{d\Omega}(Q) = \frac{1}{V}\langle \mid \sum_{k=1}^{n} b_k \, exp(i\,\boldsymbol{Q}\cdot\mathbf{R}_k) \mid^2 \rangle \tag{39}$$

here only the coherent scattering is considered, since the incoherent one contributes only a Q-independent background. A complex fluid consist usually of particles or polymer chains which can be distinguished from the solvent; it is therefore convenient to consider each particle as a scattering center. Let us then divide the scattering volume into N_c cells, each centered at a 'particle'. The position vector of the l-th nucleus in the j-th cell can be written as $\boldsymbol{R}_{j,l} = \boldsymbol{R}_j + \boldsymbol{r}_l'$, where the first vector represents the position of the center of mass of the particle j and the second is the position vector inside the j-th cell. Thus we may write:

$$\frac{d\sigma}{d\Omega}(Q) = \frac{1}{V}\langle \mid \sum_{j=1}^{N_p} exp(i\,\boldsymbol{Q}\cdot\boldsymbol{R}_j) \sum_{cell,j} b_{j,l}\, exp(i\,\boldsymbol{Q}\cdot\boldsymbol{r}_l') \mid^2 \rangle \tag{40}$$

We are therefore lead to define a form factor for each particle (cell), given by:

$$F_j(\boldsymbol{Q}) = \sum_{cell,j} b_{j,l}\, exp(i\,\boldsymbol{Q}\cdot\boldsymbol{r}_l') \tag{41}$$

In terms of this form factor the scattering cross section can be rewritten as

$$\frac{d\sigma}{d\Omega}(Q) = \frac{1}{V}\langle \mid \sum_{j=1}^{N_p} F_j(\boldsymbol{Q})\, exp(i\mathbf{Q}\cdot\boldsymbol{R}_j) \mid^2 \rangle \tag{42}$$

Since the spatial resolution of a SANS experiment $2\pi/Q_{max}$ is not enough to distinguish single atomic scatterers, we can introduce a scattering length density per particle $\rho_j(\boldsymbol{r})$:

$$\rho_j(\boldsymbol{r}) = \sum_l b_{jl}\,\delta(\boldsymbol{r} - \boldsymbol{r}_l') \tag{43}$$

and a constant average solvent scattering density ρ_s. This allows us to write the form factor in the form

$$F(\mathbf{Q}) = \int_{particle\,j} d^3r\,(\rho_j(\boldsymbol{r}) - \rho_s)\,exp(i\,\boldsymbol{Q}\cdot\boldsymbol{r}) + \int_{cell_j} d^3r\,\rho_s\,exp(i\,\boldsymbol{Q}\cdot\boldsymbol{r}) \tag{44}$$

The second term is a delta function at $\boldsymbol{Q} = 0$; therefore its contribution is outside the experimentally accessible angular window, and it can be neglected leaving

$$F(\boldsymbol{Q}) = \int_{particle_j} d^3r\,(\rho_j(\boldsymbol{r} - \rho_s)\,exp(i\,\boldsymbol{Q}\cdot\boldsymbol{r}) \tag{45}$$

From the above expression it is evident that when the scattering density of a particle is uniform, the form factor depends only on the particle shape. As mentioned before, since the it depends on the difference $\rho_{particle} - \rho_s$, by suitable variations of ρ_s it is possible to 'evidence' specific particles or subunits inside a particle if this has elements with different scattering densities.

Let us now consider the simpler case of monodisperse particles, then eq. (41) can be written as

$$\frac{d\sigma}{d\Omega}(Q) = \frac{N_p}{V}\;\mid F(Q)\mid^2\;\frac{1}{N_p}\,\langle\sum_{i=1}^{N_p}\sum_{k=1}^{N_p} exp(i\,\boldsymbol{Q}\cdot\boldsymbol{R}_i - \boldsymbol{R}_k)\rangle \tag{46}$$

This can now be put in a more compact form as

$$\frac{d\sigma}{d\Omega}(Q) = n_p\,P(Q)\,S(Q) \tag{47}$$

having defined the quantities:

$$n_p = N_p/V_P, \tag{48}$$

$$P(Q) = \mid F(Q) \mid^2, \tag{49}$$

$$S(Q) = \frac{1}{N_p} \langle \sum_{i=1}^{N_p} \sum_{k=1}^{N_p} exp(i\mathbf{Q} \cdot \boldsymbol{R}_i - \boldsymbol{R}_k) \rangle \tag{50}$$

The differential scattering cross section per unit volume is thus proportional to the particle density n_p, and depends on the product of the intraparticle form factor $P(Q)$ and the interparticle structure factor $S(Q)$. It can be shown that eq. (45) holds also for systems of n different components, and/or with moderate polydispersity, if one makes the additional assumption that the particle size and orientations are uncorrelated with the particle positions. In this case $S(Q)$ represents an averaged structure factor which can be expressed in terms of partial factors $S_{pq}(Q)$ for all possible combinations of p-th and q-th components.

VII. BIOLOGICAL STUDIES BY SANS

A. Macromolecules in Dilute Solutions

In this case we can neglect the contribution of the structure factor $S(Q)$ in eq. (47) and the small angle scattering profile gives us directly information on the overall particle (macromolecule) shape through the from factor $P(Q)$. In the range where $QR \ll 1$, if R is the particle radius, Guinier has shown that the intensity is related to the radius of gyration of the particle R_G by:

$$I(Q) = I_o \, exp\left(-\frac{Q^2 R_G^2}{3}\right) \tag{51}$$

Therefore R_G can be derived from the slope of a plot of $lnI(Q)$ vs. Q^2. If the intensity is known on an absolute scale, I_o is related to the molecular weight M of the particle.

For particles having a well defined shape (sphere, cylinder) the intensity at wider angles provides information on its shape. In the case of a homogeneous sphere of radius R the scattering intensity can be calculated analitycally as:

$$I(Q) \propto \left(3\,\frac{sin(QR) - QR\,cos(QR)}{(QR)^2}\right)^2 \tag{52}$$

Thus $I(Q)$ has a very characteristic profile with a series of well defined minima. However deviations from the ideal spherical shape (prolate od oblate ellipsoid) or any polydispersity will smear out to some extent such features.

An interesting example of a joint application of SANS and SAXS to spherical macromolecules in that of gangliosides. These biological glycolipids are made up from an oligosaccharidic chain formed by five sugar residues, and by a double hydrocarbon chain. In solution gangliosides give rise to globular aggregates (micelles) with an average radius of about 58 ÅThese micelles are seen in a different way by X-rays and neutrons: the former see the micelle has an hollow sphere, the latter as filled sphere. The two form factors are therefore drastically different, and their comparison a precise information on the relative size of lipid and saccharidic regions. At higher concentrations the data can still be interpreted with the same model adding a suitable structure factor which accounts for the inter-micellar interactions.

B. Concentrated Solutions and Complex Systems

The analysis of concentration effects, departure from ideality etc. has been extensively studied in liquid state physics and resulted in the building up of various models. The main problem in the interpretation of SANS data is the separations of the contributions to the scattering intensity coming from the form factor $P(Q)$, and from the structure factor $S(Q)$ in eq. (47). It is difficult to formulate general analysis procedures for this problem; the solution has to be adapted to the type of sample. The main useful methods are:

1. Dilution method. If the particles remain identical upon dilution, extrapolation to very low concentrations may allow to derive the form factor $P(Q)$. At finite concentrations $S(Q)$ can the be extracted.

2. Labelling method. If one can label only a point in each particle, the contrast of the rest being negligible, $S(Q)$ will dominate the scattering.

3. Calculation of the scattering profile in a model where one assumes the particle shape and their interaction potential.

Proteins are usually studied in aqueous buffered solutions to mimic *in vivo* conditions. Besides possible specific interactions between the various components, non specific interactions are present between proteins, between proteins and solvent and within the solvent. A large body of data has been published so far on protein solutions in a wide range of concentrations and of H/D contrast ratios. As an example we may recall a systematic study of lysozyme solutions at different concentrations and pH values by combined use of SLS and SANS. The measurements strongly indicate the existence of a hierarchy of structures on different scale lengths. In addition to the large-scale structural properties revealed by SLS experiments, there is also partial ordering on a molecular scale, with features similar to the large-scale ones, provided a suitable scaling of the spatial length is made. Comparison of results obtained for solutions in different chemical and physical conditions gave also some insight on the kind of interactions responsible for the observed structures.

A further class of systems extensively investigated by SANS is that of biopolymer gels; these are formed by a random biopolymer network in a solvent which is usually water. On account of their structure, rheological behaviour and transport properties they offer many opportunities for testing and extending concepts of fractality, percolation and reptation processes. An example is that of agarose gels which are commonly used as matrices for separation of DNA fragment by electrophoresis. The SANS patterns of such gels have been analysed in terms of fractal models. For an ideal monodisperse gel the scattering intensity can be expressed in terms of a correlation length *csi* (i.e. the size of non-correlated domains in the gel phase), and the fractal dimensions D inside the domain as:

$$S(Q) \propto \frac{\xi^2}{(1+(D+1)\,\xi^2 Q^2/3)^{D/2}} \tag{53}$$

For an improved model taking into account the mass polydispersity of the domains quantified by a power law with exponent τ, the scattered intensity reduced asymptotically to:

$$S(Q) \propto Q^{-D(3-\tau)} \qquad (\xi Q \ll 1) \tag{54}$$

$$S(Q) \propto Q^{-D} \qquad (\xi Q \gg 1) \tag{55}$$

Percolation cluster theories predict $\tau = 2.2$ and $D = 2.5$ near the gelation point, leading to a polydispersity smeared fractal dimension $\mu = D(3 - \tau) = 2.0$ i.e. close to what is experimentally observed for low concentration agarose gels.

Neutron scattering has been a most useful technique in the study of virus structure largely through the exploitation of the D_2O/H_2O contrast variation method. The scattering length densities of viral components are very different, hence their contribution to the scattering are minimized in different D_2O/H_2O mixtures. Proteins become 'invisible' in a mixture of $\sim$ 42 % D_2O/H_2O, RNA in 65 % D_2O/H_2O, DNA in 70 % D_2O/H_2O, abd lipids in 10 - 20 % D_2O/H_2O depending on their chemical composition. The first virus to be crystallized was tomato bushsy stunt virus (TBSV) in 1938. From this date onwards a lot of diffraction studies have been performed. In the case of SANS the measurements led to a structure which was described by a model of 4 concentric shells of different scattering length densities. The manner in which the scattering length density in each shell varied as a function of D_2O content enabled the amount of protein, RNA and water in each shell to be estimated.. An important flexibility in solution scattering is the possibility of varying the solution conditions. For TBSV particles swelling can be induced by removal of calcium or change in pH. The SANS data proved that swelling can be explained by a simple radial translation of all the viral components. The contrast variation approach has also been successfully used to study larger and more complex viruses like the influenza virus, and they allowed to build a detailed model of the virus structure.

VIII. INELASTIC AND QUASIELASTIC SCATTERING

Dynamical events in biomolecular systems occur on a very large time-scale ranging from femtoseconds to almost seconds. Within this broad interval, motions occurring in the picosecond to nanosecond time-scale are of particular interest and relevance since they cover the transition region from 'discrete' local excitations of small molecular subunits to slower processes involving cooperative motions of massive parts of the macromolecular assembly. This time window is well covered by inelastic and quasielastic neutron scattering, these techniques can therefore play a relevant role in improving the understanding of molecular motions which affect the functionality of biomolecules. The motions which contribute to the dynamics in the pico- to nanosecond region originate from a variety of processes which can be schematically classified as:

i) *Vibrational excitations.* Coherent acoustic excitations have been observed in many crystalline and paracrystalline biomolecular structures (amino acids, polypeptides, DNA) as well as in the first shells of hydration surrounding the biopolymer chains.

ii) *Side group motions.* Side groups in polypeptide and polynucleotide chains take part in the global dynamics of the structure. In nucleic acids these groups are the bases which couple the two helical strands and thus their dynamics is largely determined by that of the whole biopolymer. In proteins the situation is different since there may be also side groups relatively loosely bound for instance at the protein-buffer interface, their dynamics is then mostly determined by the interactions with the solvent.

iii) *Inter-domain motions.* These are clearly observable in proteins where relatively rigid secondary structural constituents (domains) are held together by softer parts. These motions are typically overdamped because of the large surface displacement and solvent damping involved. They are often directly connected to functional activity, for instance in enzymes where the active sites are usually located in positions at the interdomain boundaries.

iv) *Solvent-biomolecule interactions.* There is ample evidence that water in biological systems is different from bulk water. Many biological molecules posses at their surface 'specific'

binding sites for H_2O: water molecules in the first hydration shells have therefore a mobility which is highly reduced with respect to that of bulk water. As shown by recent quasielastic neutron scattering experiments on low concentration aqueous polysaccharide gels, the effects of these short-range interactions may extend over larger scale lengths modifying appreciably, even at very low biopolymer concentrations, the translational and rotational diffusion of large volumes of interstitial water.

A. Inelastic Coherent and Incoherent Scattering

The first inelastic scattering experiments experiments of biological interest were performed on DNA fibers and date back to the early 'seventies. In the past ten years the availability of large size DNA paracrystals obtained by wet-spun techniques enabled accurate inelastic scattering studies to be performed on hydrated DNA fibers in their C, A and B conformations. Overdamped and underdamped longitudinal acoustic phonons have been observed in the vicinity of a hydration dependent two-dimensional sheet of diffuse scattering perpendicular to the helix axis. In the underdamped case (DNA in B conformation) the data have been interpreted in terms of excitations propagating in a one-dimensional ordered shell of water molecules surrounding the DNA double helices. The sound velocity derived from the phonon dispersion curve (1.85 ± 0.05 km/s) is close to that usually measured in bulk water. Similar studies have also been performed on perdeuterated proteins. A full deuteration is a prerequisite for such studies, since hydrogen contributes a $Q-$independent incoherent background which may 'hide' the small signal from the phonon-like excitations.

Useful dynamic information can however be also obtained from hydrogenous biomolecules. In this case what is measured is an 'average' vibrational property i.e. a protons vibrational density of states $G(\omega)$. In the case of myoglobin this was done after separating contributions from elastic, quasielastic and inelastic scattering according to:

$$S(Q,\omega,T) = e^{-Q^2U^2_{vib}(T)} \cdot [A(Q,T)\delta(\omega) + S_{qel}(Q,\omega,T) + S_{vib}(Q,\omega,T)] \qquad (56)$$

where the first term is a Debye-Waller (DW) factor and $A(Q,\omega,T)$ is the elastic incoherent structure factor (EISF). The density of states $G(\omega)$ was then obtained as the limit:

$$G(\omega) = \lim_{Q\to 0} \frac{6\omega}{\hbar Q^2}(e^{\hbar\omega/k_BT} - 1)\, S_{vib}(Q,\omega) \tag{57}$$

This was done under the assumption that $G(\omega)$ is temperature independent and that the temperature dependence of the inelastic scattering occurs only in the DW and Bose factors as in a harmonic system. The obtained $G(\omega)$ curves, at temperatures $\leq$ 180 K show a Debye-like behaviour (i.e. $G(\omega) \propto \omega^2$) only in the low frequency region (below 20 cm^{-1}). A small but significant enhancement above the Debye form is seen centered at $\sim$ 25 cm^{-1} has been interpreted in terms of a fractal behaviour ($G(\omega) \propto \omega^{d-1}$, where d is the spectral dimension of the fractal structure). The crossover from phonon to fracton regime takes place at $\omega_c \sim 25$ cm^{-1}, a frequency which corresponds to a scale length of $\sim$ 40 Å, approximately the size of the myoglobin molecule.

B. Quasielastic Incoherent Scattering

The diffusive motion of particles in soft matter systems can not be quantized, since the motion is random and the energies are continuously distributed. Therefore the inelastic scattering cross section (eq. (28)) is no longer given by a sum of $\delta-$functions at finite momentum and energy transfers as in the case of solids. There is instead a contribution centered at zero energy transfer with a characteristic quasi-elastic linewidth proportional to the diffusivity of the particles. To relate this quasi-elastic neutron scattering (QENS) to particular stochastic particle motions, it is at first convenient to rewrite the general expression for the double-differential cross section in eq. 20 in terms of the so-called 'dynamic structure factor' $S(\boldsymbol{Q},\omega)$:

$$\frac{d^2\sigma}{d\Omega d\omega} = \frac{\boldsymbol{K}_f}{\boldsymbol{K}_i}\frac{N}{4\pi}\left\{\sigma_{coh}\, S_{coh}(\boldsymbol{Q},\omega) + \sigma_{inc}\, S_{inc}(\boldsymbol{Q},\omega)\right\} \tag{58}$$

The cross sections σ_{coh} and σ_{inc} are properties of the neutron-nucleus interactions. The dynamic structure factors are given by

$$S_{coh}(\boldsymbol{Q},\omega) = \frac{1}{2\pi\hbar N}\int exp(-i\omega t)\,\langle\sum_{lk} exp(i\,\boldsymbol{Q}\cdot\boldsymbol{R}_l(0))\,exp(i\,\boldsymbol{Q}\cdot\boldsymbol{R}_k(t))\rangle\,dt \tag{59}$$

$$S_{inc}(\boldsymbol{Q},\omega) = \frac{1}{2\pi\hbar N}\int exp(-i\omega t)\,\langle\sum_{l} exp(i\,\boldsymbol{Q}\cdot\boldsymbol{R}_l(0))\,exp(i\,\boldsymbol{Q}\cdot\boldsymbol{R}_l(t))\rangle\,dt \tag{60}$$

The dynamic structure factors represent the space and time Fourier-transforms of correlation functions:

$$S_{coh}(\boldsymbol{Q},\omega) = \frac{1}{2\pi\hbar}\int G(\boldsymbol{r},t)\,exp\;i(\boldsymbol{Q}\cdot\boldsymbol{r}-\omega t)\;dt \tag{61}$$

$$S_{inc}(\boldsymbol{Q},\omega) = \frac{1}{2\pi\hbar}\int G_s(\boldsymbol{r},t)\,exp\;i(\boldsymbol{Q}\cdot\boldsymbol{r}-\omega t)\;dt \tag{62}$$

Here $G(\boldsymbol{r},t)$ and $G_s(\boldsymbol{r},t)$ are pair- and self-correlation functions respectively. This formalism was introduced by Van Hove. It is not generally possible to derive the Van Hove correlation functions by space and time Fourier inversion of the experimental data. One usually formulates a model for the correlation functions, then the dynamic structure factors are calculated and compared to the data. In the following we will quote three simple examples which can provide a guideline for the understanding of more complex particle motions:

- Free flying particle In this case a Gaussian shaped self-correlation function is assumed in space. The Fourier transform is then:

$$S(\boldsymbol{Q},\omega) = \left(\frac{M\beta}{2\pi\hbar^2Q^2}\right)^{1/2} exp(-\omega^2 M\beta/2Q^2) \tag{63}$$

where $\beta = 1/K_BT$. Therefore $S(\boldsymbol{Q},\omega)$ for the free flying particle has a Gaussian shape with a FWHM of:

$$\Gamma = 2\hbar\sqrt{\frac{2ln2}{m\beta}}\;Q \tag{64}$$

- Diffusive motion The basic equation governing random diffusion is Fick's law, which leads to a Lorentzian shaped incoherent dynamic structure factor:

$$S(\boldsymbol{Q},\omega) = \frac{1}{\pi\hbar}\;\frac{DQ^2}{(DQ^2)+\omega^2} \tag{65}$$

its width (FWHM) exhibits a typical parabolic increase as a function of Q

$$\Gamma_{inc} = 2\hbar\,D\,Q^2 \tag{66}$$

- Translational jump diffusion This can be seen as a hopping type motion on random, radially distributed sites. The dynamic structure factor then turns out to be Lorentzian shaped as in the case of simple diffusion:

$$S_{trans}(\boldsymbol{Q},\omega) = \frac{1}{\pi\hbar}\,\frac{\Gamma_t(Q)}{\Gamma_t^2(Q)+\omega^2} \tag{67}$$

its width (FWHM) depends upon two parameters: a translational diffusion coefficient D_t, and a residence time between jumps τ_o

$$\Gamma_t = \frac{D_t Q^2}{1 + D_t Q^2 \tau_o} \tag{68}$$

Let us now analyse some examples of quasielastic scattering studies of biological macromolecules. A general description of protein dynamics in terms of glassy system models has been proposed by Frauenfelder in the late 'seventies. This idea is mainly based on results of viscoelastic measurements which show a steplike increase in Young's modulus of highly hydrated proteins in the temperature range 220 - 250 K, as well as from studies of the kinetics of CO rebinding to myoglobin (flash photolysis experiments) which are non-exponential in time and non-Arrhenius in temperature. A simple explanation of the non-exponential ligand binding invokes the existence of conformational substates arranged in hierarchy. A protein in a given state can assume a very large number of structurally very similar substates with slightly different activation enthalpies. Below a critical temperature transitions between substates are absent and the system is 'frozen' in a particular substate, in this way a non-ergodic behaviour is obtained.

The fact that proteins show some features typical of glasses has also suggested the use of glassy state models to explain the temperature behaviour of QENS. Elastic scans of hydrated myoglobin have been performed at the ILL reactor in Grenoble. Between 4 and 180 K the elastic intensity has the gaussian form typical for an harmonic solid where the vibrational atomic motions are described by a DW factor. Near 200 K an extra decrease of the elastic intensity indicates the onset of new degrees of freedom. At the same time a broad quasielastic component develops between 0 and 3 meV. By combining the data obtained using different

spectrometers the authors have been able to extract the energy and Q dependence of the quasielastic scattering component.

A similar study has been recently performed on superoxide dismutase a protein which is globular like myoglobin, but has a much more rigid polypeptide scaffolding. The behaviour of the elastic scattering intensity (Debye-Waller factor) turns out to be similar to that of myoglobin. On the other hand the quasielastic contribution to the spectrum is much smaller and at room temperature is below 25 %. this reflects the overall higher rigidity of this protein.

Membranes are fundamental elements of all living cells; they act not only as passive protective screens, but perform also important active functions controlling transport of molecules and ions across them. Plasma membranes are complex multilayered systems, their main components are a smectic A layer (the lipid/protein bilayer) and a quasi two-dimensional macromolecular network (the so called cytoskeleton) loosely coupled together. The lipid bilayer itself is a complicated multicomponent system made up from about 100 different lipid components which differ in the details of the hydrocarbon chain and of the polar heads. These lipid molecules are amphiphillic and thus favour formation of bilayer sheets in which their polar heads are located on both external sides of the double layer. QENS offers many unique advantages for studying the lipid bilayer dynamics: i) selective deuteration techniques can be used to single out the dynamics of specific parts or units; ii) the measure of the EISF can provide a clear information on the spatial extension of motions allowing one to distinguish between free in-plane diffusion and spatially restricted dynamics; iii) by making use of highly oriented samples it is possible to differentiate between in-plane and out-of-plane motions. For this purpose the dynamic structure factor has to be measured for different directions of Q with respect to the layer orientation.

Among phospholipid bilayers, dipalmitoylphosphatidylcholine (DPPC) in the most popular and largely studied one because of its high stability and also because it has a transition from a low temperature solid (gel) phase (L_β) to a liquid crystalline (L_α) phase occurring at about 60°C (the exact value depends on the water content of the sample). It is therefore easy to study the bilayer dynamics at temperatures above and below this transition. In

the last few years QENS studies in this field have greatly benefited from the availability of highly oriented stacks of lipid bilayers obtained by deposition of DPPA vesicles on thin silicon substrates. A high degree of orientation of the lipid molecules (mosaic spread = $\pm 1.25°$) was obtained by annealing treatments at 100°C in a humidity controlled atmosphere. In-plane and out-of-plane dynamics have been studied at different temperatures. Spectra were fitted to a superposition of an elastic line (for motions restricted in space) and one or two Lorentzian quasielastic components. In the fluid phase the analysis of the EISF for both parallel and perpendicular orientations of the bilayer with respect to **Q** indicates that the proton motion is essentially isotropic and agrees with a model of in- and out-of-plane diffusion within a restricted volume. In order to get a good fitting it is necessary to assume a distribution of volumes for the different protons with mean displacements ranging from $\sim$ 0.6 Å for protons near the glycerol backbone to $\sim$ 8 Å for protons close to the chain ends.

The role of water in biological systems has been object of extensive studies. A large variety of results and interpretations which are often strongly technique-dependent have appeared in the literature There is however a general consensus on the fact that the mobility and organization of water molecules near biomolecular surfaces markedly differ from that of 'bulk' water. Many biomolecules have specific binding sites for water so that the first hydration shell around a biomolecule is made up from H_2O molecules which are irrotationally bound (primary hydration water), and their dynamics closely follows that of the whole biomolecular skeleton. Macromolecule-water interactions are short range, however their integrated effects propagate to relatively large scale lengths so that the dynamic properties of interstitial water are significantly different from those of pure H_2O. Biopolymer-water interactions can be studied in a wide range of concentrations in polysaccharide gels. A systematic study on these gels has been carried out in the past few years at the ILL (Grenoble) and at the at the ISIS spallation source (U.K.). In the gel state agarose molecules are arranged in a double helical secondary structure, and hydrogen-bonded bundles of 10-50 double helices form a random 3D network of fairly stiff rods connected through junction zones; this network through van der Waals volume and H-bonding interactions is capable of slowing

down significantly the diffusive motions of vicinal water layers. Having in mind this picture of the gel structure, the QFNS spectra obtained from hydrogenous gels can be fitted to an incoherent structure factor made up of three contributions arising from water layers with different mobilities:

$$S(Q,\omega) = f^I W^I \delta(\omega) + f^{II} W^{II} S_{rot}(Q,\omega) + f^{III} W^{III} \cdot [\mathcal{S}_{trans}(Q,\omega) \otimes S_{rot}(Q,\omega)] \quad (69)$$

The population factors (satisfying $f^I + f^{II} + f^{III} = 1$) refer to: a first shell of hydration of irrotationally bound protons (I), protons capable of performing hindered rotational motions, but site bound up to times $\sim 10^{-8}$ sec. (II), protons belonging to the interstitial aqueous phase (III); W^i are the respective DW factors. The broader component which originates from the contributions of type-II and type-III protons has a width which markedly depends upon temperature and gel concentration. Its Q-dependence can be described reasonably well by the random jump diffusion model discussed previously A detailed analysis of the temperature dependence of the diffusive parameters indicates that water diffusivity in gels can be described according to percolation models and MD simulations which picture water as a continually restructuring gel-like random network of H-bonded molecules, and predict the rapid forming and breaking of H-bonded water clusters.

IX. REFERENCES

General textbooks

[1] J.M. Carpenter, and W.B. Yelon, 'Neutron Scattering - Methods of Experimental Physics, Vol 23A and 23B, edited by K. Sköld and D.L. Price, Academic Press, N. Y. 1986.

[2] S.W. Lowesey, 'Theory of Neutron Scattering from Condensed Matter', Clarendon Press, Oxford 1984.

[3] C.G. Windsor, 'Pulsed Neutron Scattering', Taylor & francis, London 1981.

[4] HERCULES, 'Neutron and Sinchrotron radiation for Condensed Matter Studies', Vols. I, II, III, Springer-Verlag and Les Editions de Physique, Berlin and Les Ulis 1994.

[5] O. Glatter, and O. Kratky, O., 'Small Angle X-ray Scattering', Academic Press, N.Y., 1982.

[6] A. Guinier, and G. Fournet, 'Small Angle Scattering of X-Rays', Wiley, N.Y. 1955.

[7] L.A. Feigin, D.I. Svergun, 'Structure Analysis by Small Angle X-Ray and Neutron Scattering', Plenum Press, N.Y. 1987.

[8] M. Bée 'Quasielastic Neutron Scattering', Adam Hilger, Bristol, 1988.

Properties of the neutron.

mass	$m_n = 1.008664924\ (14)\ u$
spin	$s = 1/2$
magnetic moment	$\mu_n = 1.91304275\ (45)\ \mu_N$
electric charge	$q_n = (-0.4 \pm 1.1) \cdot 10^{-21}\ e$
electric charge: mean square radius	$r_n = 0.11 \pm 0.02$ fm
electric dipole moment	$d_n = (-0.7 \pm 0.4) \cdot 10^{-21}$ e cm
polarizability	$\alpha = (1.2 \pm 1.0) \cdot 10^{-3}$ fm^3
β decay of a free neutron	$n \rightarrow p^+ + e^- + \nu$
life time	$\tau = 888 \pm 3$ s
half life	$T_{1/2} = \tau \ln 2 = 615 \pm 3$ s

Some reactor sources.

reactors	country	power	flux	sources		guides	instruments
		MW	$n\,cm^{-2}s^{-1}$	cold	hot		
ILL	F	57	$15 \cdot 10^{14}$	2	1	10	30 (60)
Orphée	F	14	$3 \cdot 10^{14}$	2	1	7	21
Jülich	D	23	$2 \cdot 10^{14}$	1		15	
Berlin	D	10	$2 \cdot 10^{14}$	1		5	12
Risö	DK	10	$0.35 \cdot 10^{14}$	1		8	
Oak Ridge	US	100	$15 \cdot 10^{14}$	-			
BNL	US	60	$10 \cdot 10^{14}$	1			
NIST	US	20		1		7	
JAERI	Japan	20	$2 \cdot 10^{14}$	1		5	20
Bombay	India	100	$2 \cdot 10^{14}$	(1)	(1)	2	14
IBR-2	Russia	2	10^{13}				
	pulsed	1500	$(3 \cdot 10^{16})$	5--25 Hz			9
PIK	Russia	100	$12 \cdot 10^{14}$	1		6	construction
ANS	US	200	$8 \cdot 10^{15}$	1		12	project

Table 5. Some spallation sources.

source	country	MeV	μA	target	$n\,s^{-1}$	freq. Hz	instr.
IPNS	US	500	15	U	$1.7 \cdot 10^{15}$	30	7 (+4)
LANSCE	US	800	100	W	$9.3 \cdot 10^{15}$	12	9
KENS	Japan	500	110	W	$5.6 \cdot 10^{14}$	20	7
ISIS	GB	800	110 (200)	U	$3.7 \cdot 10^{16}$	50	12+ν+μ
SINQ	CH	590	2000	Pb-Bi	$1.1 \cdot 10^{17}$	continuous	constr.

Nuclear reactions for neutron production.

E (MeV)	particle	target		neutron energy	price MeV/n	heat MeV/n
100	e	W	bremsstr. + photo effect	evaporation	3000	
0.2	d	T		14 MeV	2500	
35	d	^{9}Be		evaporation	1200	
35	d	^{7}Li		evaporation	730	
1000	p	Pb	spallation	cascade	50	50
1000	p	^{238}U	spallation	< 1000 ~2MeV	25	55
-	n	^{235}U	fission	~2 MeV		200
-	D	T	fusion	14 MeV		3

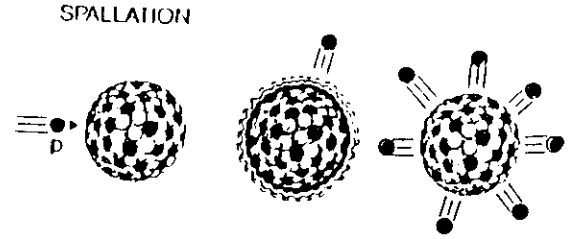

— (a) Fission reaction: a thermal neutron is absorbed by a ^{235}U nucleus, which splits into fission fragments and evaporates off a few neutrons with energies of 1 to 2 MeV. (b) Spallation: a high-energy proton (~1 GeV) chops pieces off a heavy nucleus. Twenty to forty neutrons are evaporated with energies of typically a few MeV.

1. Cœur
2. Réflecteur d'eau lourde
3. Piscine
4. Circuit primaire
5. Circuit secondaire
6. Circuit d'eau lourde
7. Mécanismes de commande des barres de contrôle
8. Echangeur
9. Pompe
10. Bâche de vidange de la piscine
11. Source froide
12. Source chaude
13. Canal tangentiel
14. Hall des expérimentateurs
15. Guide à neutrons
16. Hall pile

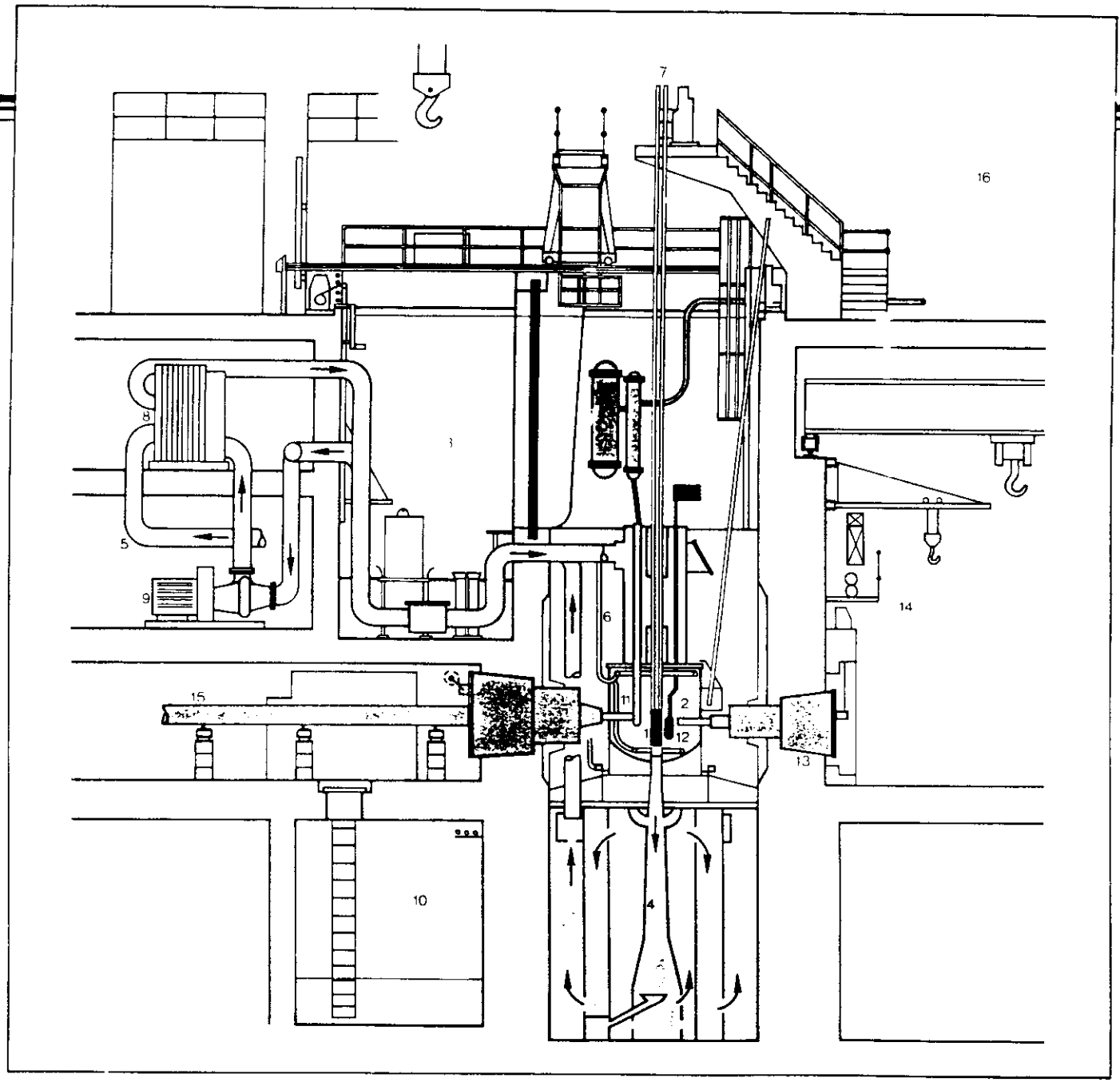

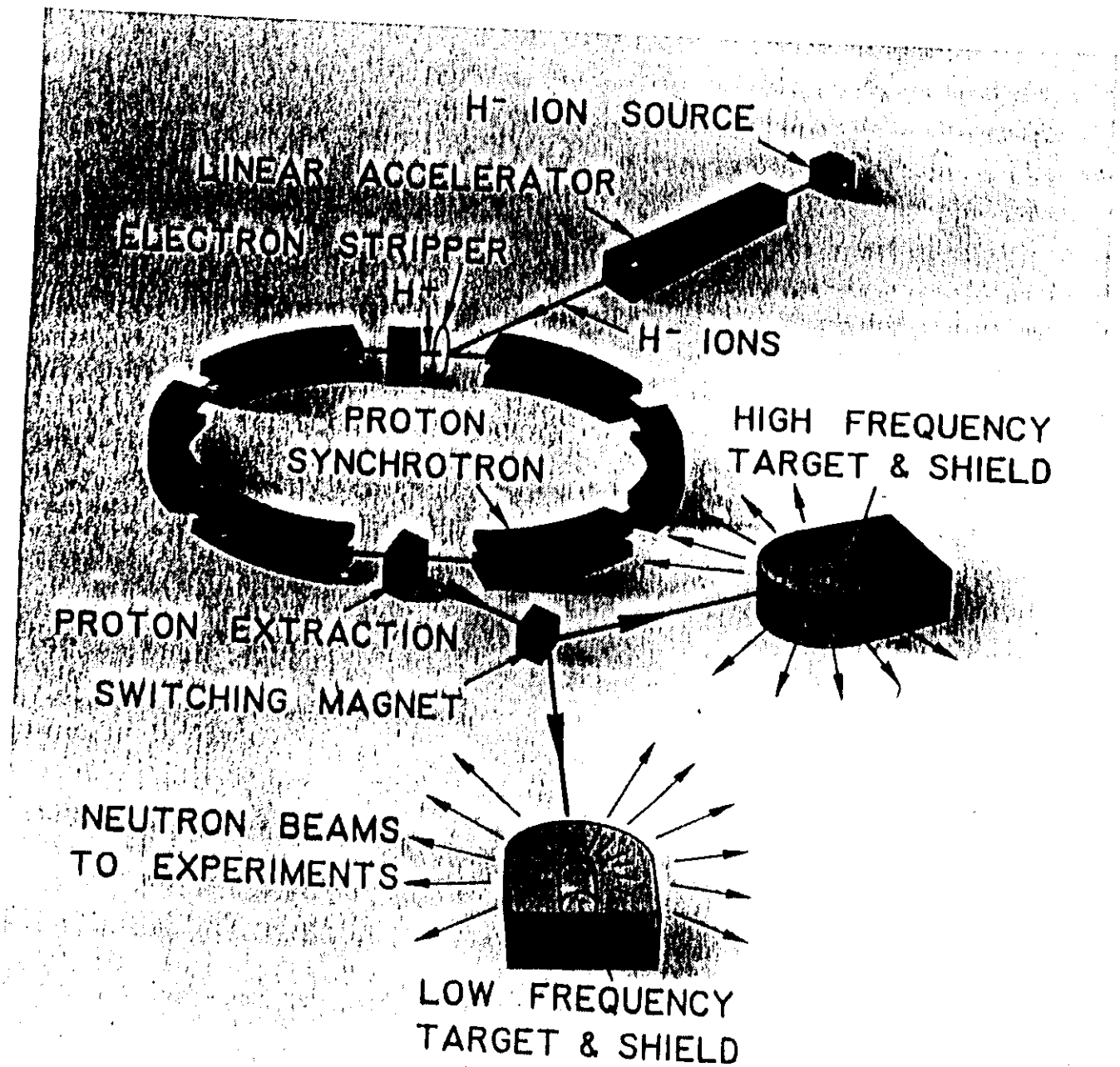

Schematic arrangment of a proton accelerator-driven pulsed neutron source.

Layout of the ISIS experimental hall

. Nuclear reactions used to detect (and absorb) neutrons. The cross sections are given in barns (1 barn = 10^{-28} m^2).

Reaction	Cross section for 25 meV *n*	Particles generated	Energy (MeV)	Total Energy (MeV)
$n + {}^3He$	5333 b	p	0.57	0.77
		^3T	0.20	
$n + {}^6Li$	941 b	^3T	2.74	4.79
		^4He	2.05	
$n + {}^{10}B$	3838 b	^4He	1.47	2.30
		^7Li	0.83	
		γ	0.48 (93%)	
$n + {}^{235}U$	681 b	fission		1--2

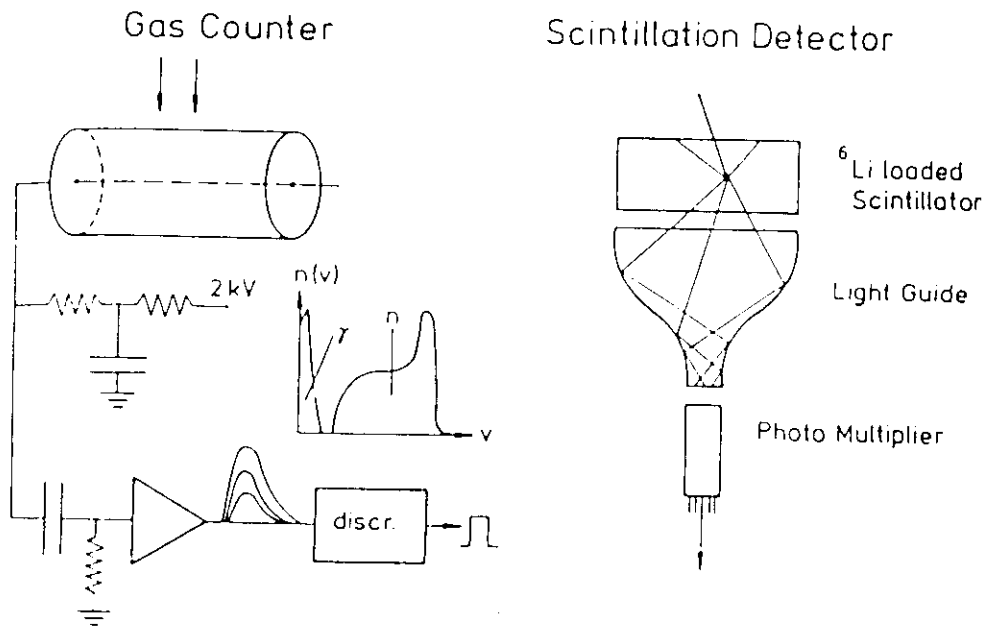

— Neutron detectors. (a) Gas proportional counter: Neutrons are absorbed in ^3He or $^{10}BF_3$ gas. The charged reaction products ionize the gas, and the electrons are multiplied. (b) Scintillation detector: A solid scintillator loaded with ^6Li transforms the reaction energy released by the absorbed neutron into many photons, which in turn are fed into a photomultiplier.

$$\left(\frac{d^2\sigma}{d\Omega\, d\omega}\right) = \frac{|\vec{k}_f|}{|\vec{k}_i|}\frac{\sigma}{4\pi} N \left[\frac{1}{2\pi\hbar}\frac{1}{N}\sum_{\ell}\sum_{k}\int \langle e^{i\vec{Q}\cdot(\vec{R}_k(0)-\vec{R}_\ell(t))}\rangle e^{-i\omega t}\, dt\right]$$

$$S(\vec{Q},\omega)$$

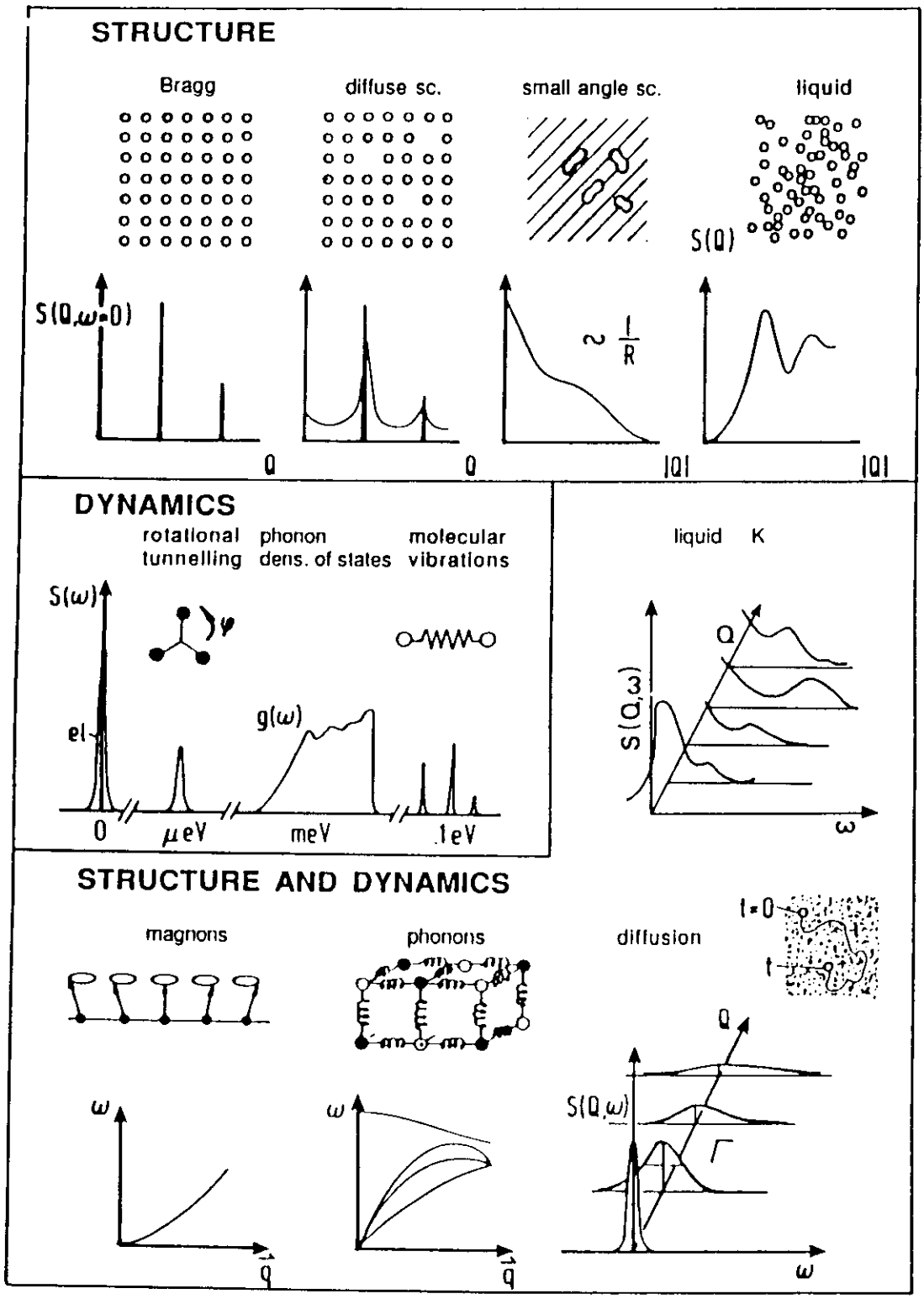

— Classification of the scattering function S(Q,ω). The structure (periodic crystals, defects, clusters, or spatial correlations in a liquid) is reflected in a more or less pronounced Q-dependence of the scattering S(Q,ω=0). The motion of localized items gives rise to inelasticity S(ω) at any Q. Propagating (collective) motions r(t) give Q-dependent frequencies in S(Q,ω).

Diffusion élastique

Un premier dispositif, appelé monochromateur, sélectionne parmi les neutrons sortant du réacteur ceux dont l'énergie et la longueur d'onde conviennent le mieux à l'expérience. Le faisceau sélectionné est dirigé sur l'échantillon à étudier, disposé sur un support orientable, et dont l'orientation est repérée avec précision. C'est l'intensité du rayonnement diffusé alors sous différents angles par l'échantillon qui est mesurée à l'aide d'un détecteur mobile. Le spectromètre ainsi constitué permet l'étude de la structure de la matière, c'est-à-dire la description de l'arrangement des atomes et molécules qui constituent les solides, les liquides et les gaz. Il permet aussi l'étude des structures magnétiques, c'est-à-dire l'arrangement des aimants "microscopiques", les atomes magnétiques qui composent les matériaux aimantés.

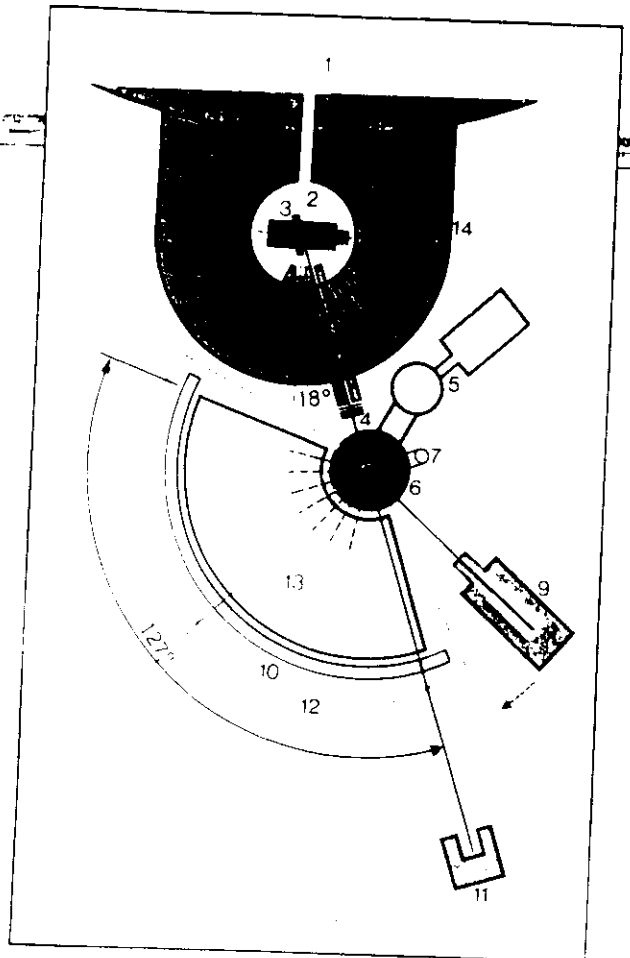

1. Réacteur ORPHEE
2. Faisceau polycinétique
3. Monochromateur
4. Faisceau monochromatique
5. Pompes
6. Enceinte étanche
7. Ligne H F
8. Axe échantillon
9. Compteur
10. Multicompteur 640 cellules
11. Piège à neutrons
12. Protection multicompteur
13. Boite à hélium
14. Protection biologique

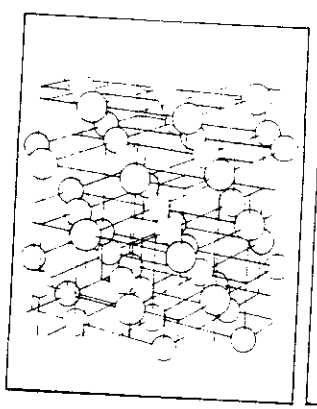

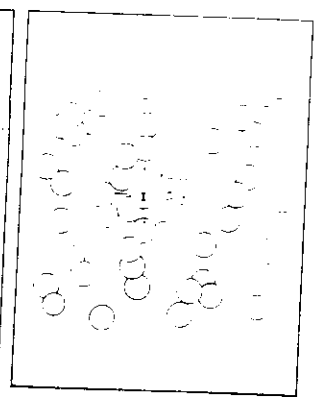

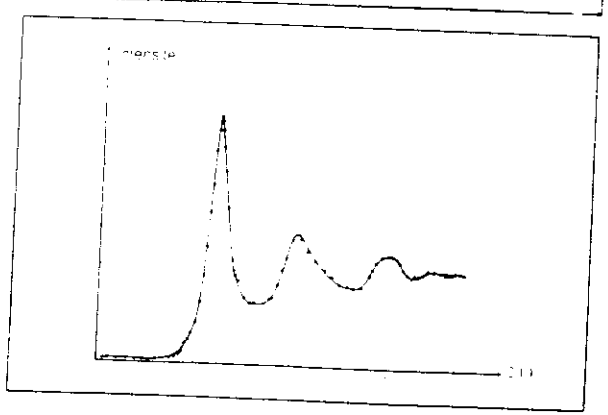

a) Un métal à l'état solide est caractérisé par une structure régulière à 3 dimensions. Chaque cercle représente un atome du métal.

b) Le même métal à l'état liquide bien que paraissant désorganisé est caractérisé par un ordre à courte distance très marqué. Cet ordre local est responsable d'un certain nombre de propriétés du liquide. Il est révélé et mesuré par l'interprétation de l'intensité diffusée.

c) Intensité diffusée après normalisation par le nickel à l'état liquide à la température de 1550°C.

Diffusion inélastique

Dans ce cas, une partie du rayonnement sélectionné par le monochromateur est diffusée par l'échantillon étudié en ayant changé de longueur d'onde et donc d'énergie. C'est ce changement de longueur d'onde que l'on mesure avec un dispositif approprié. On tire de cette mesure beaucoup d'informations et, par exemple, des renseignements sur les mouvements des atomes qui constituent l'échantillon. Ces mouvements incessants qui sont liés à la température des corps sont responsables, entre autres, des propriétés thermiques et des changements de structures que subit la matière sous certaines conditions extérieures : température, pression.

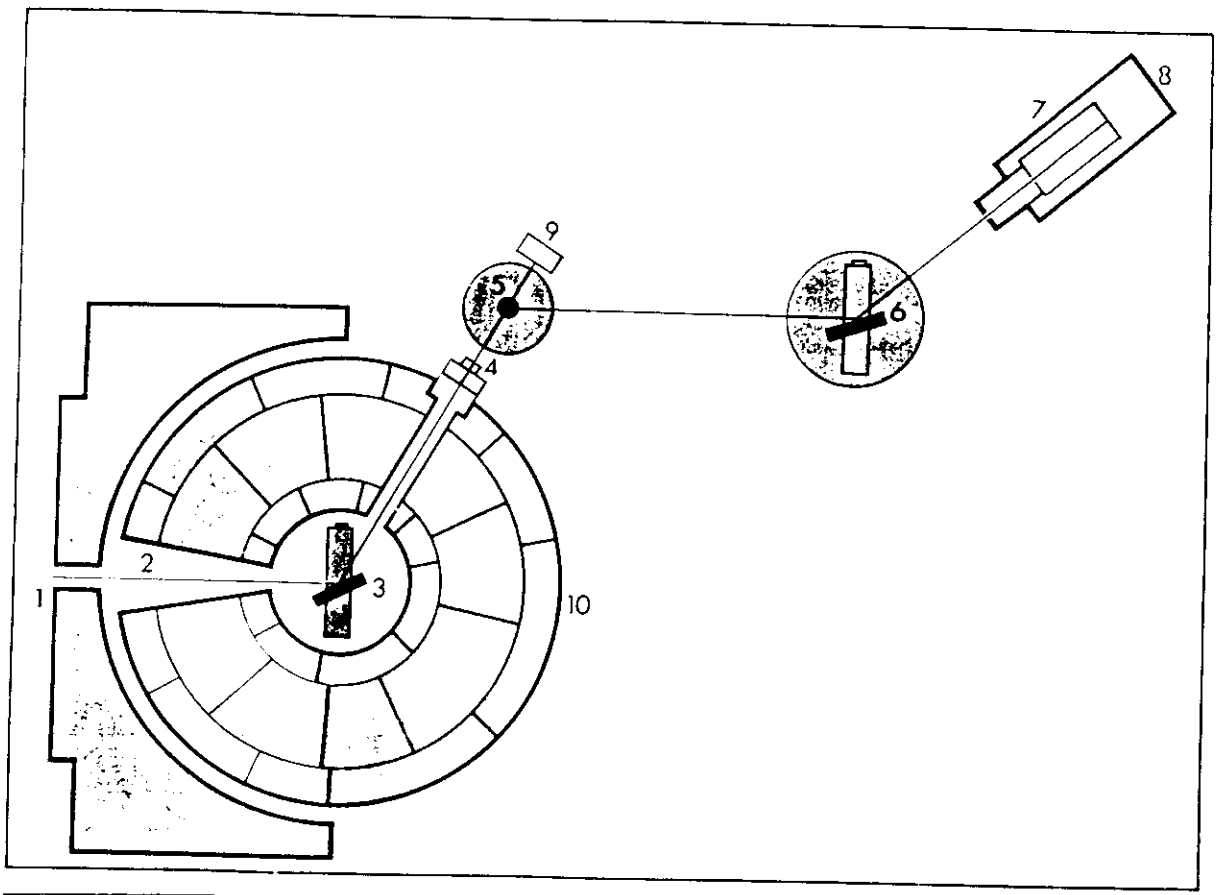

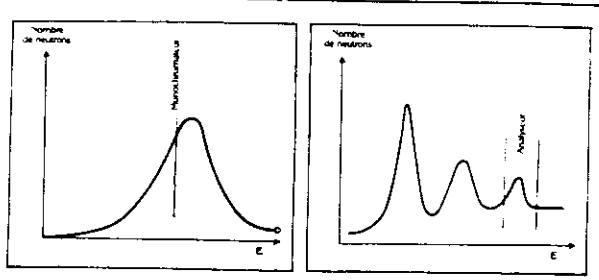

1. Réacteur ORPHÉE
2. Faisceau polycinétique
3. Monochromateur
4. Faisceau monochromatique
5. Axe échantillon
6. Analyseur
7. Détecteur
8. Protection du détecteur
9. Piège
10. Protection biologique.

Le monochromateur sélectionne dans le rayonnement incident les neutrons d'énergie E, (a). Dans l'échantillon ils subissent des variations d'énergie. Le spectre diffusé présente alors des pics dont l'énergie est mesurée à l'aide d'un second monochromateur, appelé analyseur, couplé à un détecteur (b).

- First neutron diffraction study of myoglobin:
  B.P. Schoenborn, Nature 224, 143 (1969)
  (scattering density maps at ≈ 2.0 Å resolution)

- Identification of the catalytic base in the active site of trypsin
  A.A. Kossiakoff, S.A. Spencer, Nature 288, 414 (1980)

The catalytic site holds 3 invariant residues:

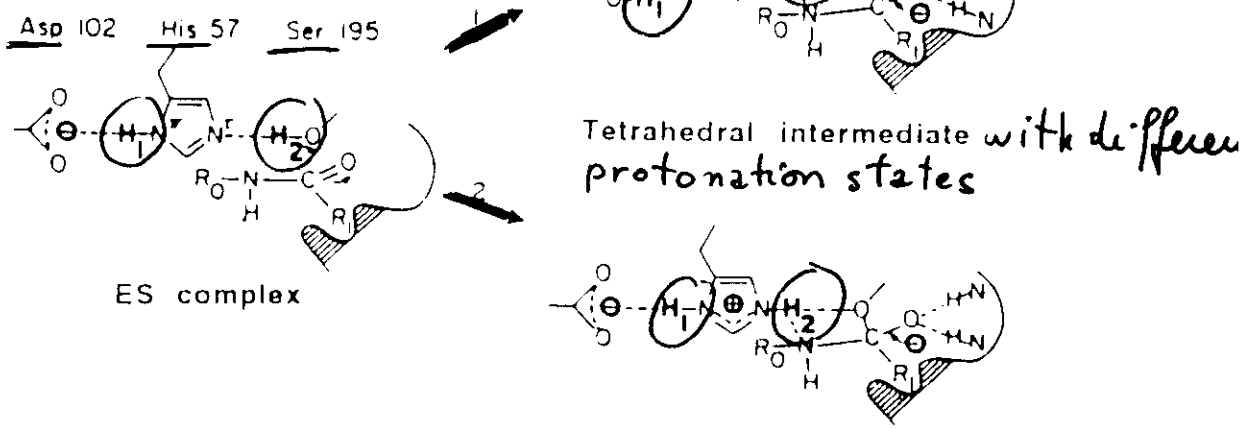

— Two models for the intermediary state in the protein hydrolysis by trypsin

Model 2 is the most likely one.

Looking for water:

- H.F.J. Savage in 'Water in Biological Macromolecules' (E. Westhof Ed.), MacMillan Press, London 19

One of the solvent regions in a crystal hydrate of coenzyme B_{12}

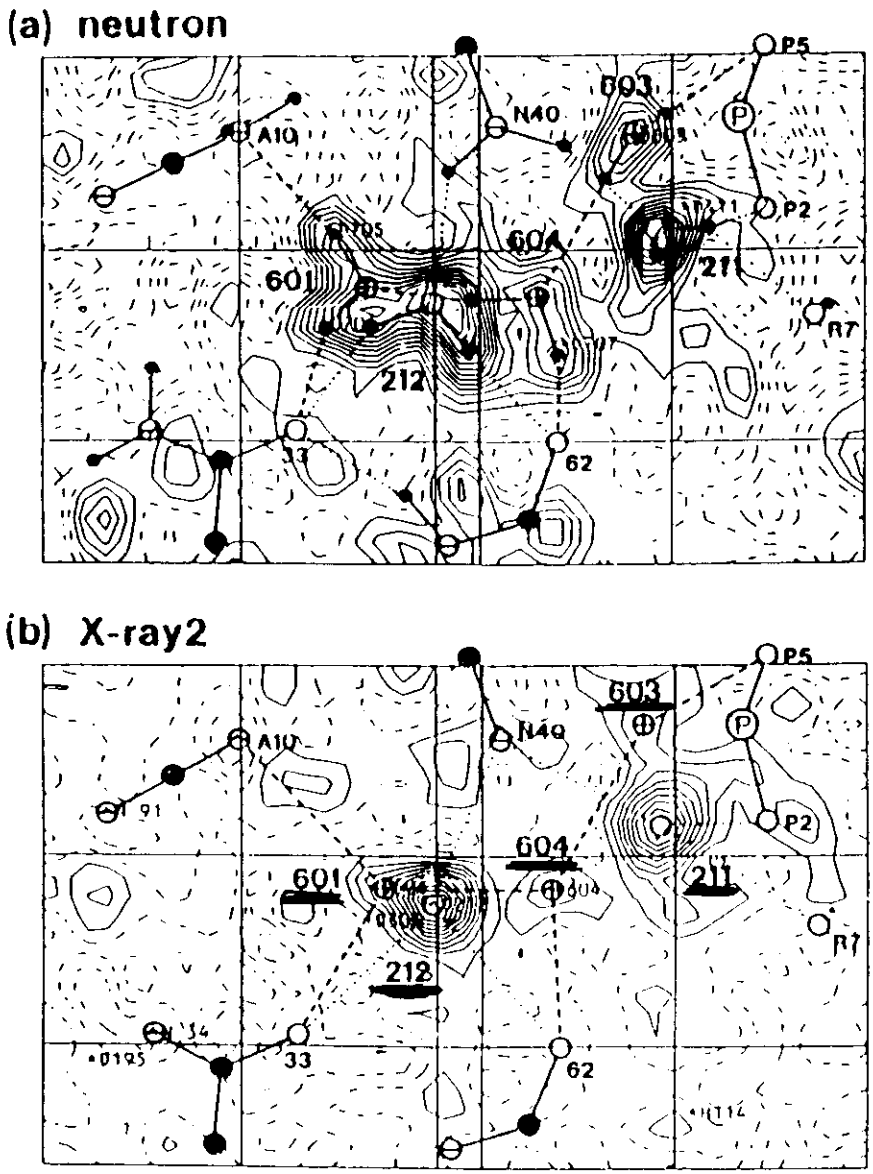

Solvent density around disordered side-chain N40 of the coenzyme B_{12} molecule: (*a*) neutron, (*b*) X-ray $F_o - F_c$ difference Fourier maps (the alternative position for the side-chain N640 is not shown, but lies ~1.8 Å behind N40. Two partially occupied solvent networks are present—
network A: waters 211 and 212; occupancies, 0.9(X-ray), 0.6(neutron);
network B: waters 601, 603, 604; occupancies, 0.1(X-ray), 0.4(neutron)

• H.F.J. Savage in 'Water in Biological Macromolecules' (E. Westhof Ed.), MacMillan Press, London 199.

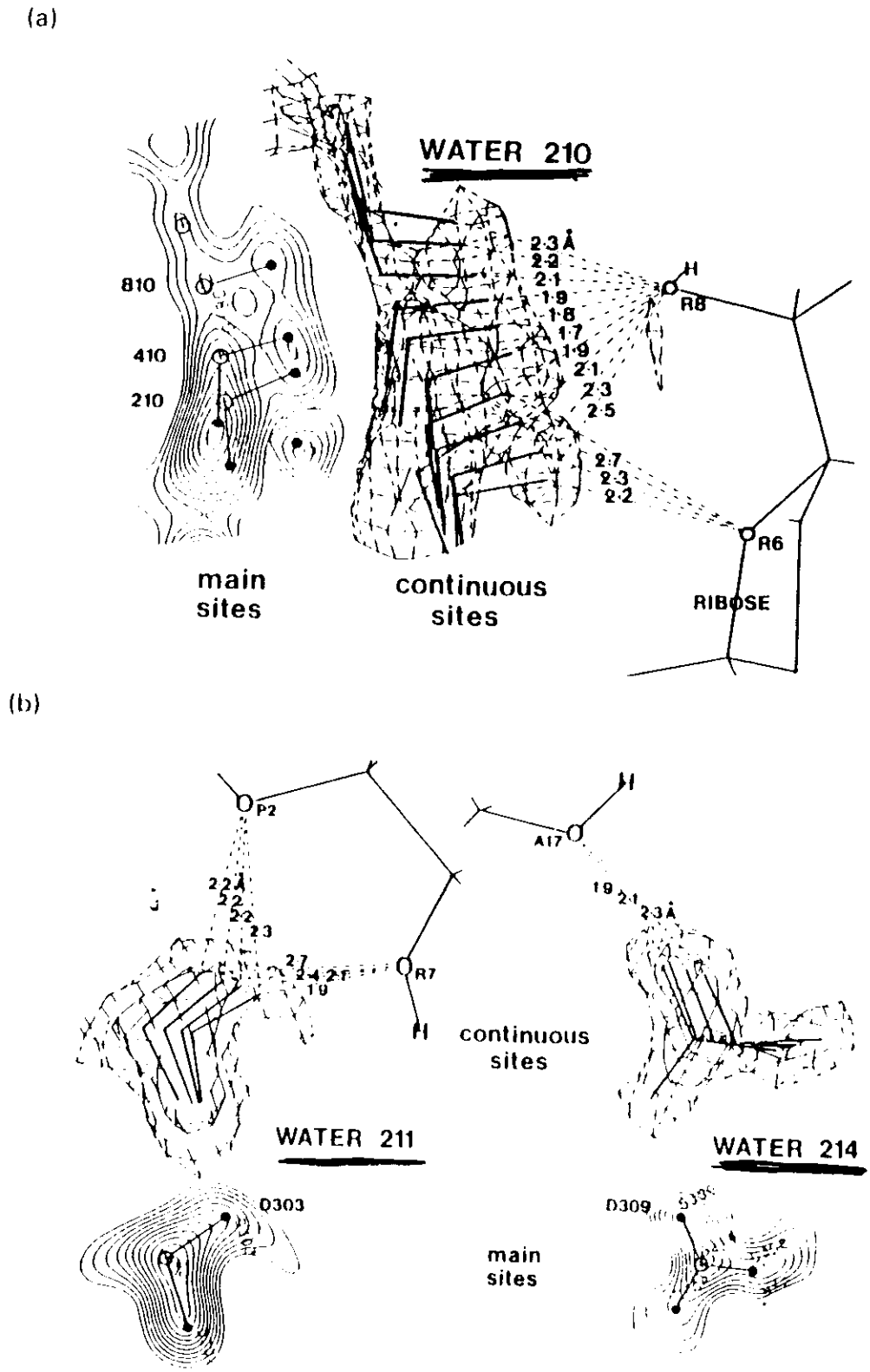

Interpretation of solvent regions in coenzyme B_{12} structural analysis: (*a*) over the 210 solvent region, (*b*) over the 211 and 214 solvent regions. 'Main' sites initially assigned to well-defined solvent density. 'Continuous' sites assigned to the elongated and diffuse regions of solvent density

W. Fuller et al., Physica B 156 & 157 (1989) 468.

D_2O H_2O Difference

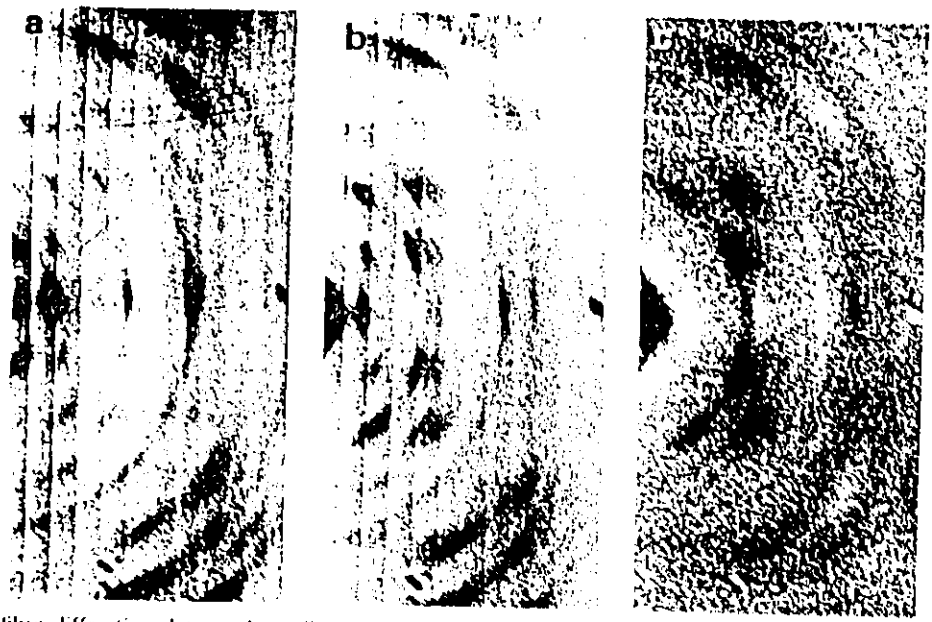

. Neutron fibre diffraction data on layer lines 0 to 5 from the D conformation of poly [d(A-T)].poly [d(A-T)]. (a) D_2O surrounding the DNA. (b) H_2O surrounding the DNA. (c) Difference between (a) and (b).

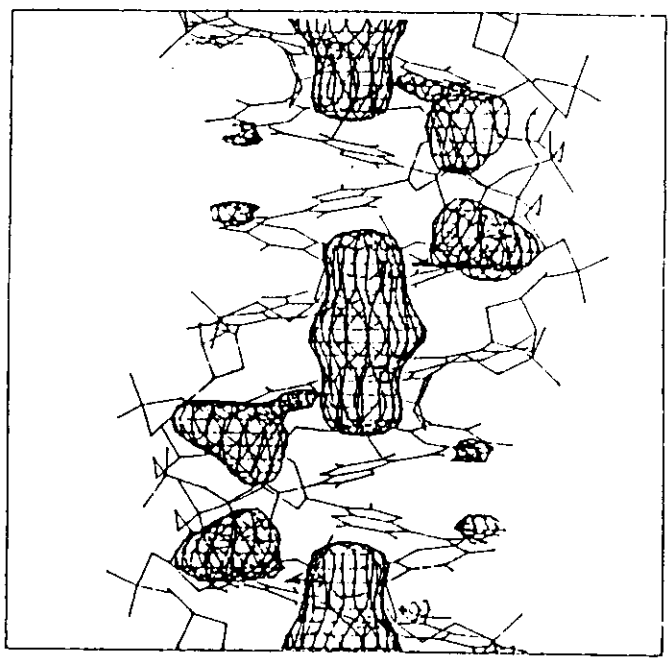

Fourier difference synthesis indicating the location of water closely associated with the D form of the DNA double-helix. The molecular skeleton shows the covalent bonds of the DNA. The synthesis is three-dimensional and is viewed perpendicular to the helix axis.

P. Langan et al., J. Biomolec. Struct & Dynamics, 10, 489 (1992)

Density maps in $F_d - F_h$

Family I
Peaks occurring between O1 oxygens of neighbouring residues

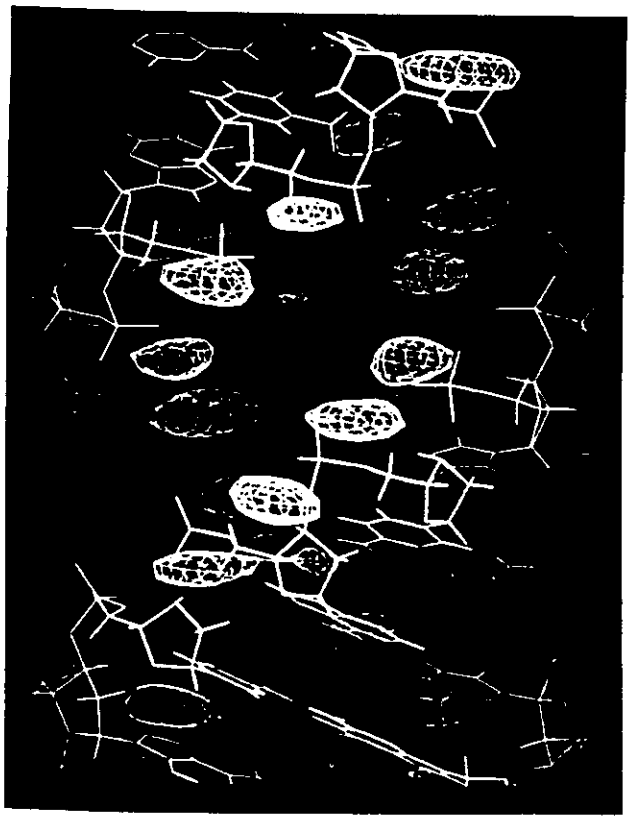

Family II
Peaks occurring between O2 oxygens of successive residues

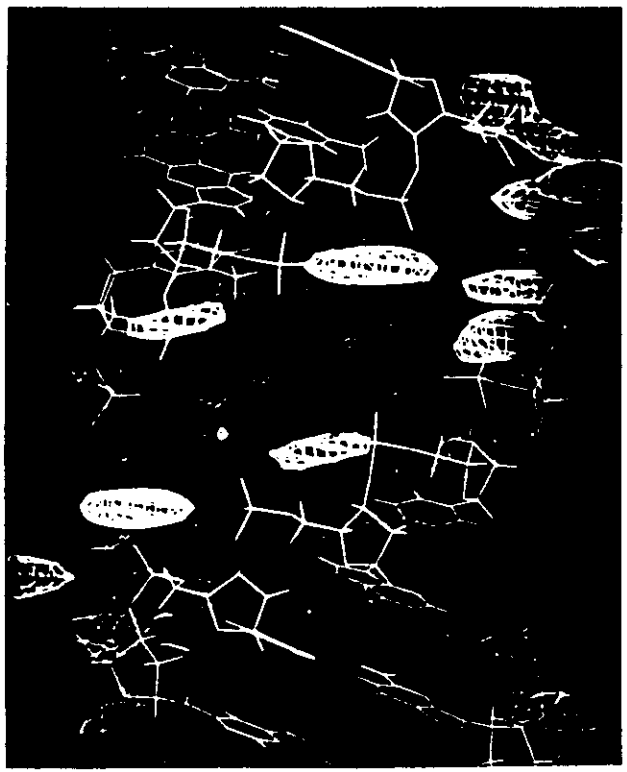

Family III
Peaks occurring in positions between the sugar and minor groove base edges.

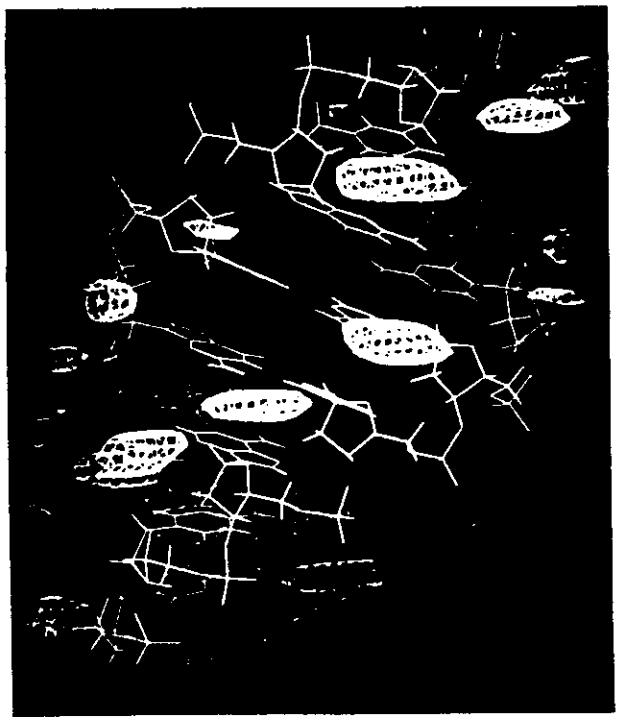

A-DNA

Local dynamics:

- A.A. Rossiakoff in 'Neutrons in biology' (B.P. Schoenborn Ed.), Plenum Press, 1984.

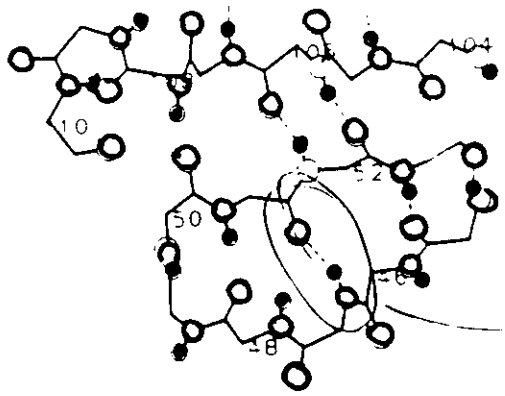

- Unexchanged H
- Deuterium

— Main chain of trypsin from residue 47 to 52, showing the internal hydrogen bonding

A 'zipper type' motion can be excluded

Low resolution studies:

For these studies long wavelenghts (8-10Å°) are best suited.

- Low resolution contrast variation experiment to locate the lipids in the micelle cavity.
  - R. Raag et al, J. Mol. Biol. 200, 353 (1988)

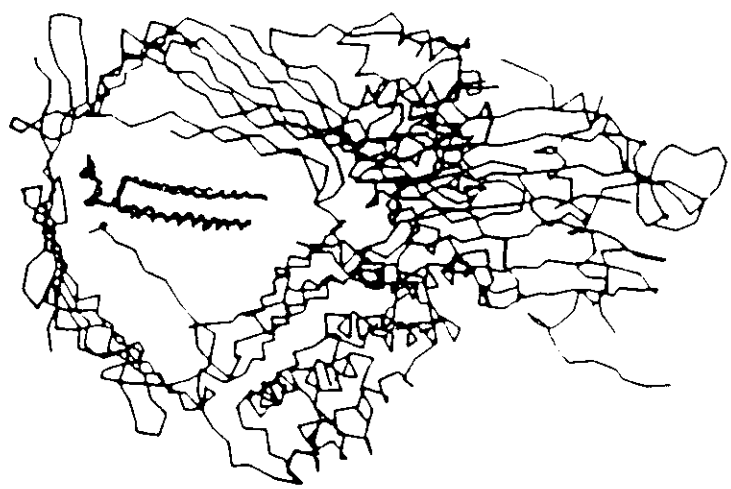

— Polypeptide chain of lipovitellin. (a protein of about 32000 D) which binds lipids

Schematic representation of the type of samples investigated by small angle scattering.

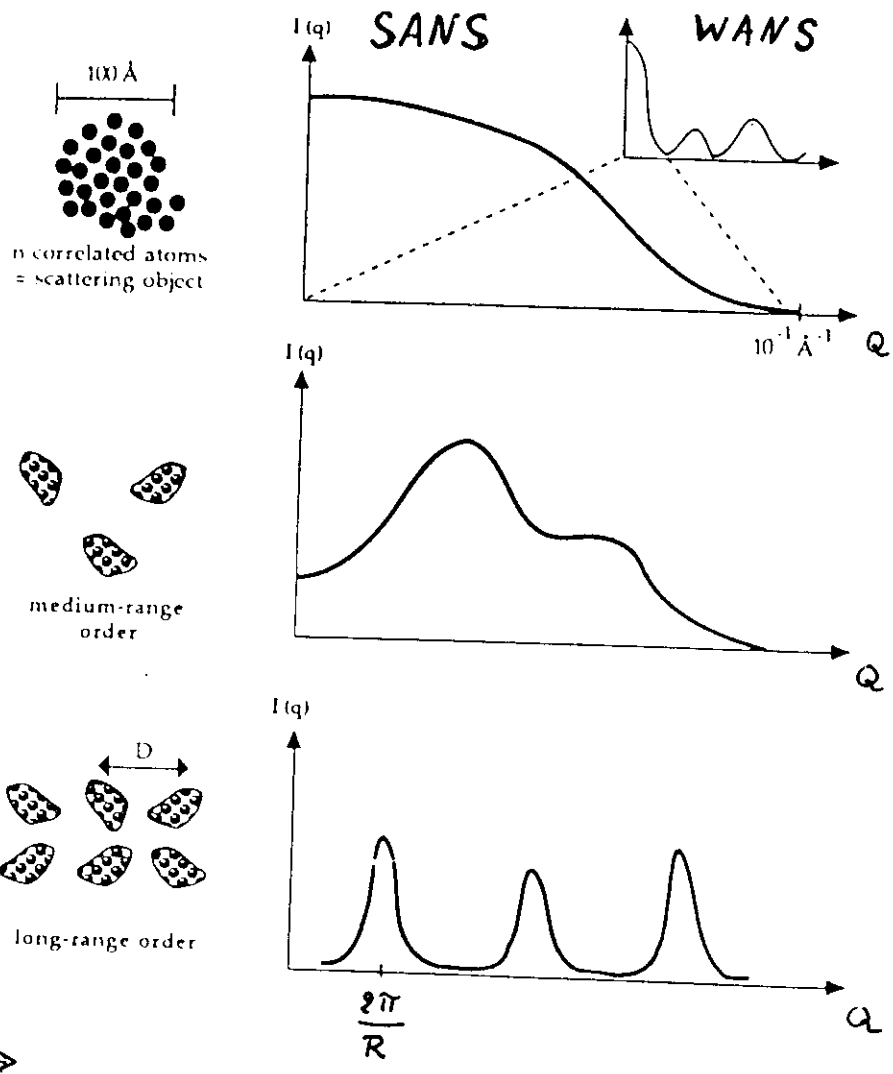

$$\vec{Q} = \vec{K_i} - \vec{K_f}$$

$$|\vec{K_i}| = |\vec{K_f}| = \frac{2\pi}{\lambda}$$

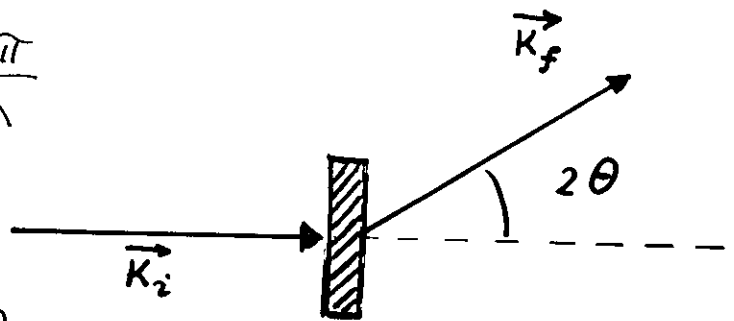

$$Q = \frac{4\pi n}{\lambda} \sin\theta$$

n = refractive index of the sample

Typical configuration of a SANS instrument

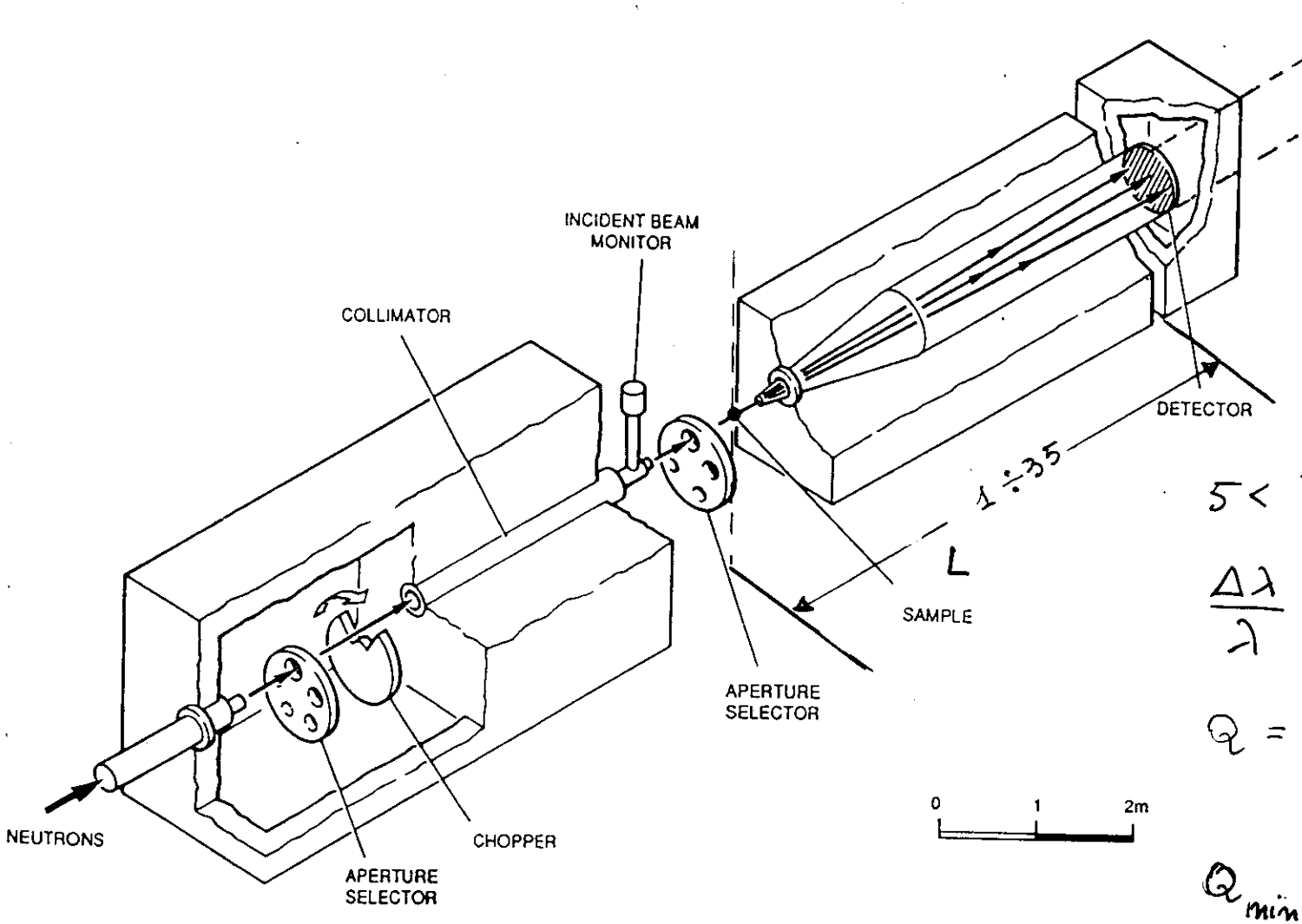

$5 < \lambda < 20$ Å

$\frac{\Delta\lambda}{\lambda} \simeq 10\%$

$Q = \frac{2\pi}{\lambda} \sin\theta \simeq \frac{2\pi}{\lambda} \frac{d}{L}$

$Q_{min} \simeq 10^{-3}$ Å^{-1}

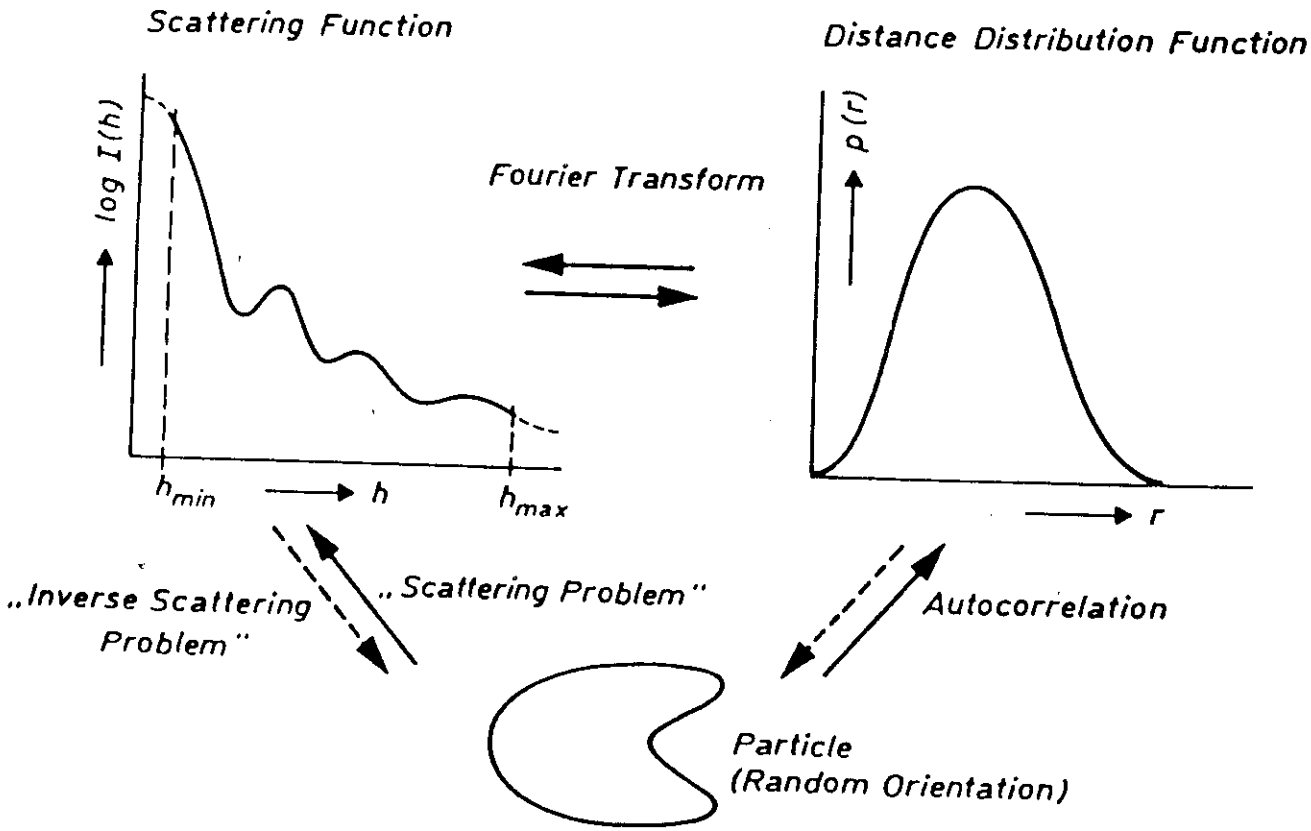

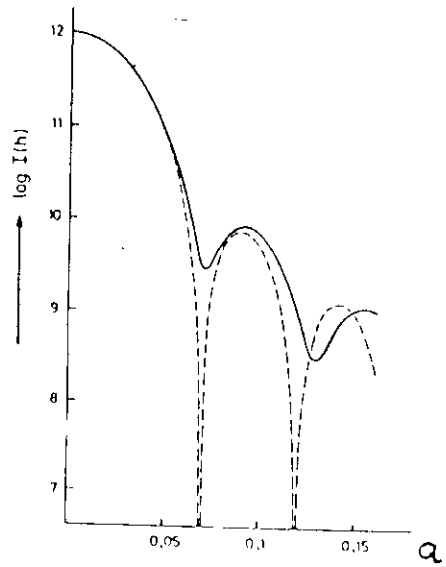

Comparison of the scattering functions of a sphere (– – – –) and a cube (———) with the same radius of gyration.

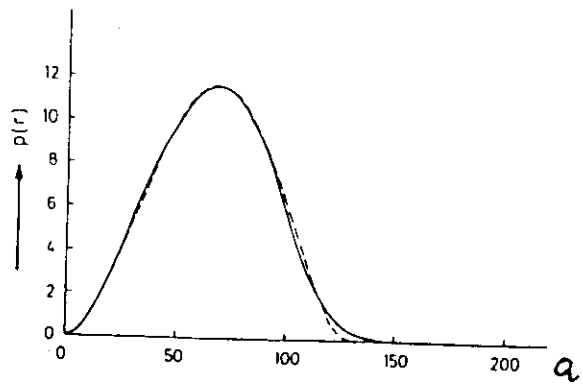

Distance distribution function of a sphere (– – – –) and a cube (———) with the same radius of gyration and the same scattering intensity at zero angle.

SANS & SAXS study of GM1 ganglioside.
L. Cantù, M. Corti, D. Acquotti, S. Sonnino, J. Phys (France) IV, 3, (1993), C1-57

GM1 ganglioside

→ oligosaccharide unit (5 sugars)

→ double hydrocarbon chain

Diluted system

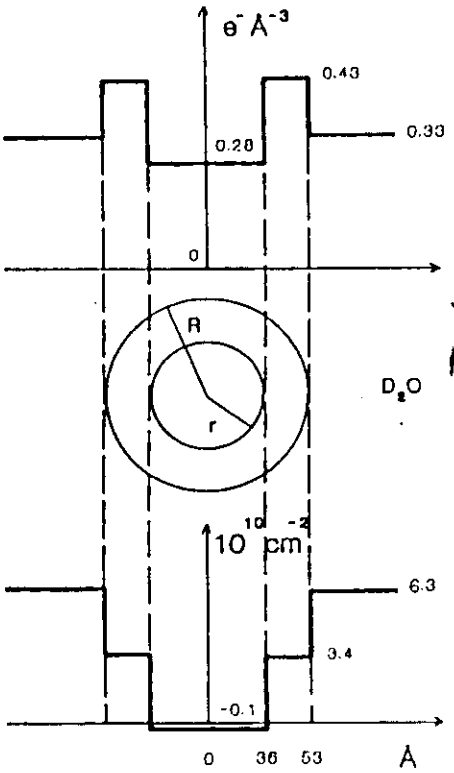

r = 36 Å
R = 58 Å

X-ray →

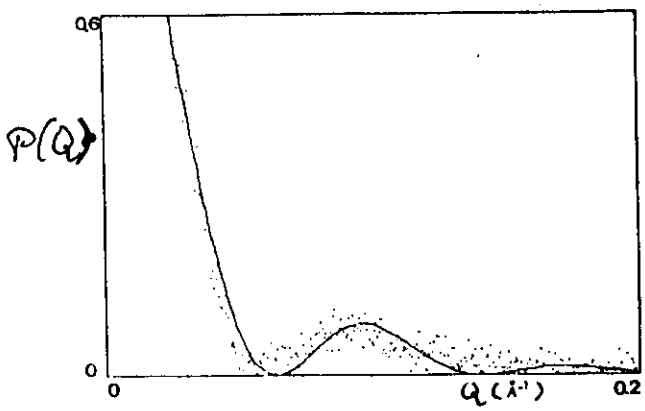

Neutrons →

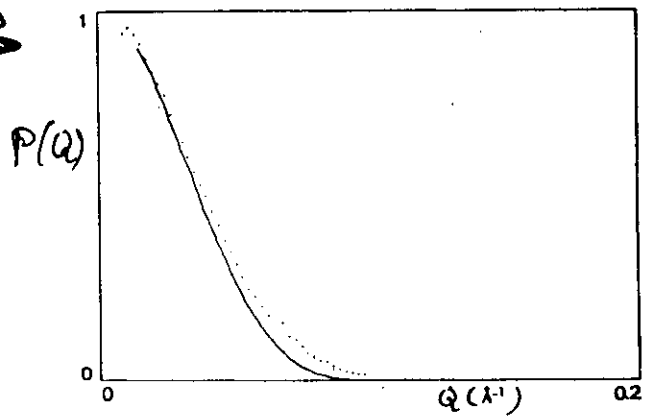

Concentrated system

GM1 15% solution

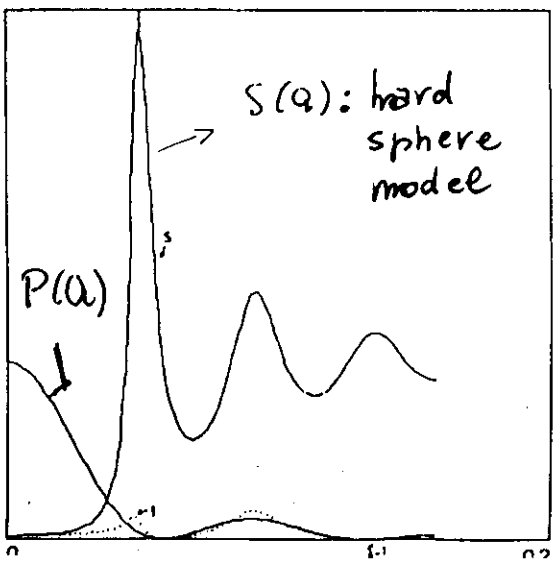

P(Q)·S(Q) ≈

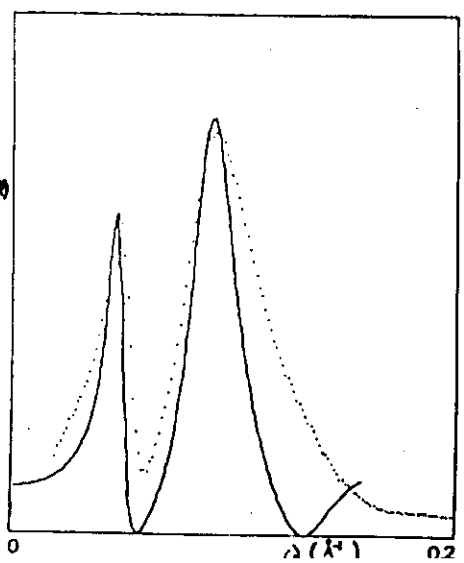

Protein solutions.

R. Giordano, A. Grasso, J. Teixeira, F. Wanderlingh, U. Wanderlingh, Phys. Rev. A43, (1991) 6894

Myoglobin solutions at different concentration, T & pH.

- Adopted model for $S(Q)$ $S(Q) = 2\,\dfrac{1 - e^{-Q^2\sigma^2/4}\cdot\cos(QL)}{1 - 2e^{-Q^2\sigma^2}\cos(QL) + e^{-Q^2\sigma^2/2}}$
- $P(Q) \equiv$ prolate ellipsoid (axes: 13.5 Å, 21.9 Å)

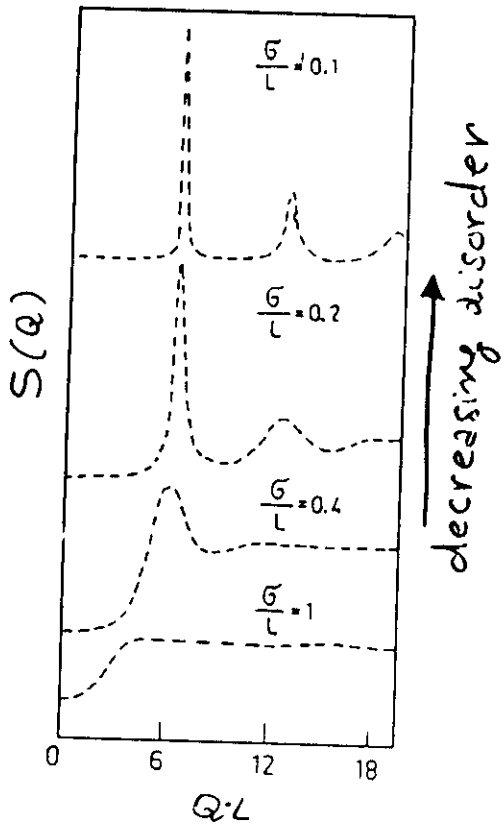

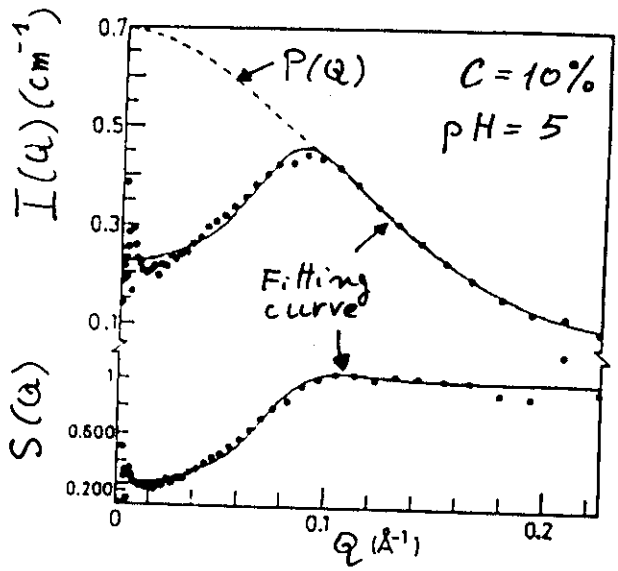

Concentration (wt. %)	L(Å)	σ(Å)	A	S(0)	d(Å)
0.0	55.6	39.3	0.36	0.25	77.3
0.10	51.4	35.7	0.63	0.24	61.3
0.15	46.1	36.5	0.83	0.31	53.6
0.20	48.7	40.6	0.87	0.35	48.7

d = average distance from concentrati
$\propto n^{-1/3}$

Effect of pH

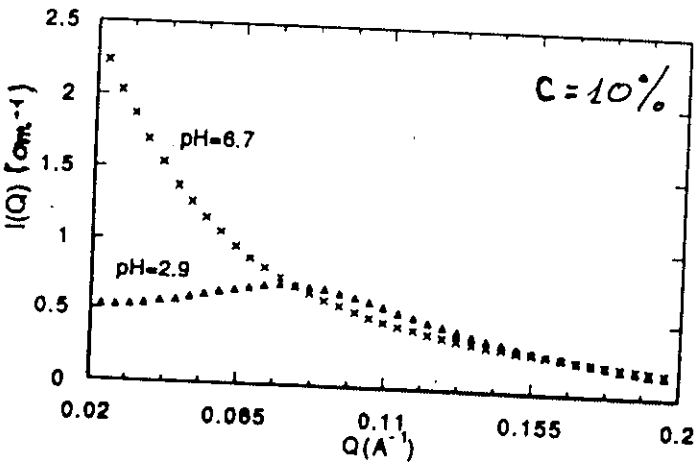

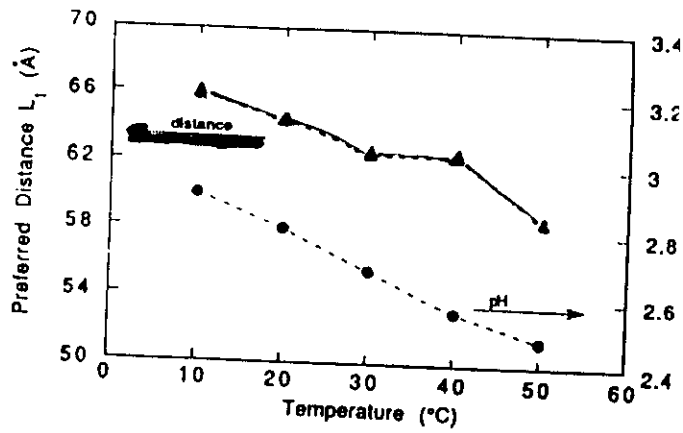

SANS from polysaccharide gels.

- A. Deriu et al. J. Physique IV, 3, C1-237 (1993).

a)

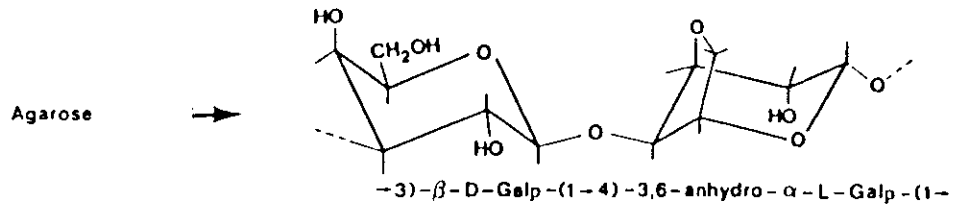

b)

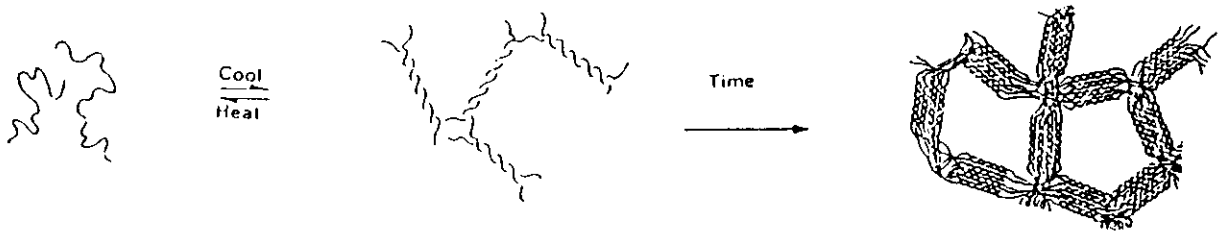

a) The agarose dimer. b) Sketch of the process leading to the hierarchical structure of agarose gels.

$$S(Q) \propto \frac{\xi^2}{(1+(D+1)\xi^2 Q^2/3)^{D/2}}$$

$$S(Q) \propto \varphi^{-D(3-\tau)} \quad (\xi Q \ll 1)$$

$$S(Q) \propto \varphi^{-D} \quad (\xi Q \gg 1)$$

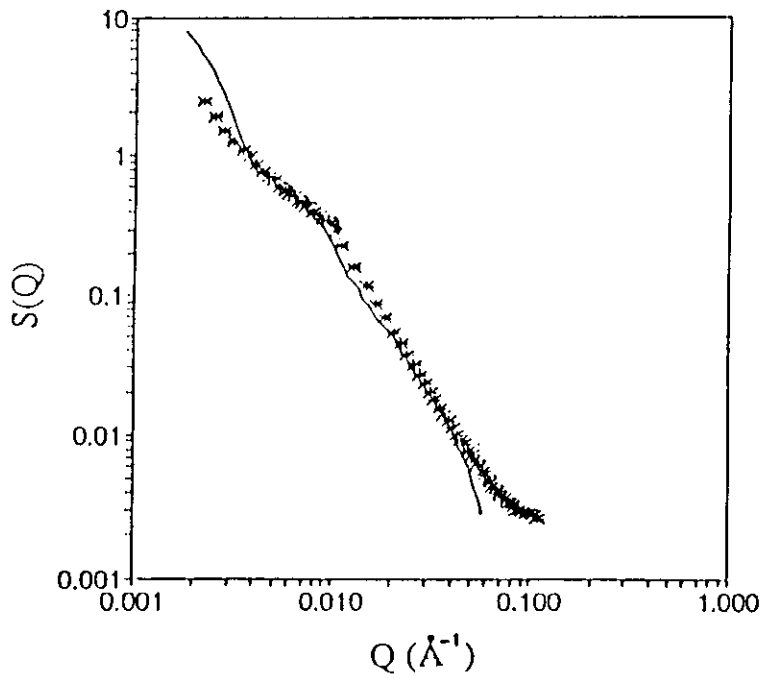

log-log plot of the intensity scattered by a set of fully D_2O exchanged gel samples with concentration C = 0.01.

Percolation theories predict $\tau = 2.2$ $D = 2.5$ near the gelation point leading to $\mu = D(3-\tau) = 2.0$

TBSV - B. Jacrot in 'Comprehensive Virology' 17 (Ed. Fraenkel-Conrat and R.R. Wagner), Plenum, N.Y. 1981

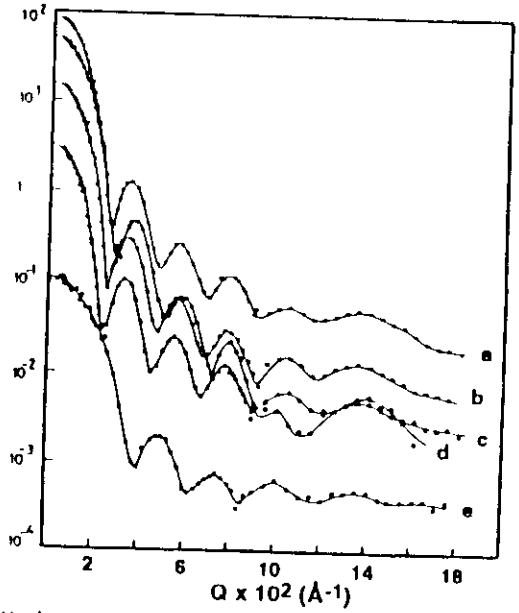

— Neutron scattering curves from TBSV solutions of various D_2O / H_2O content (A) 100%, (B) 68%, (C) 55%, (D) 0%, (E) 41%.

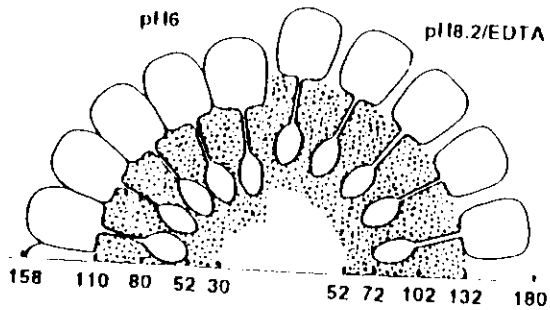

— Schematic representation of the radial distribution of protein and RNA in compact and swollen TBSV.

Influenza virus - S. Cusack, Inst. Phys. Conf. Ser. 64 Sect. 4, 351 (1982).

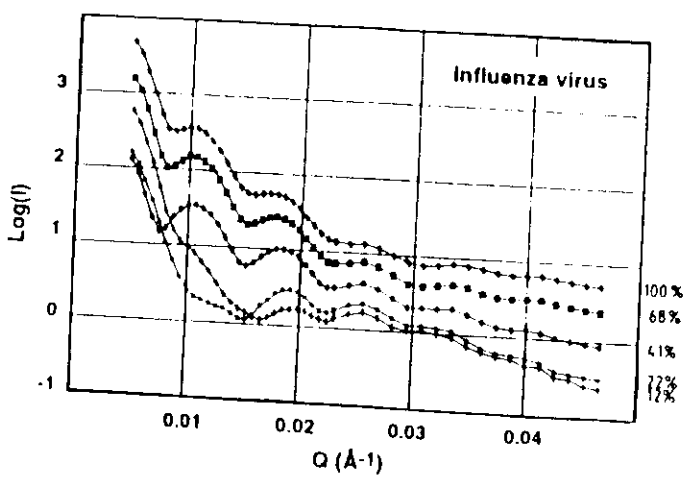

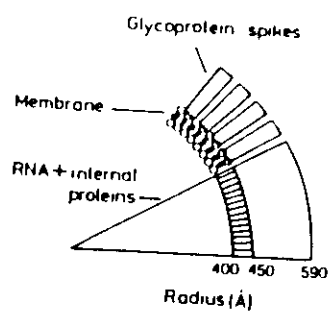

— (a) Neutron scattering curves from solutions of influenza virus in different D_2O/H_2O mixtures as indicated. (b) Low resolution model of the influenza virus as deduced from the small angle scattering curves.

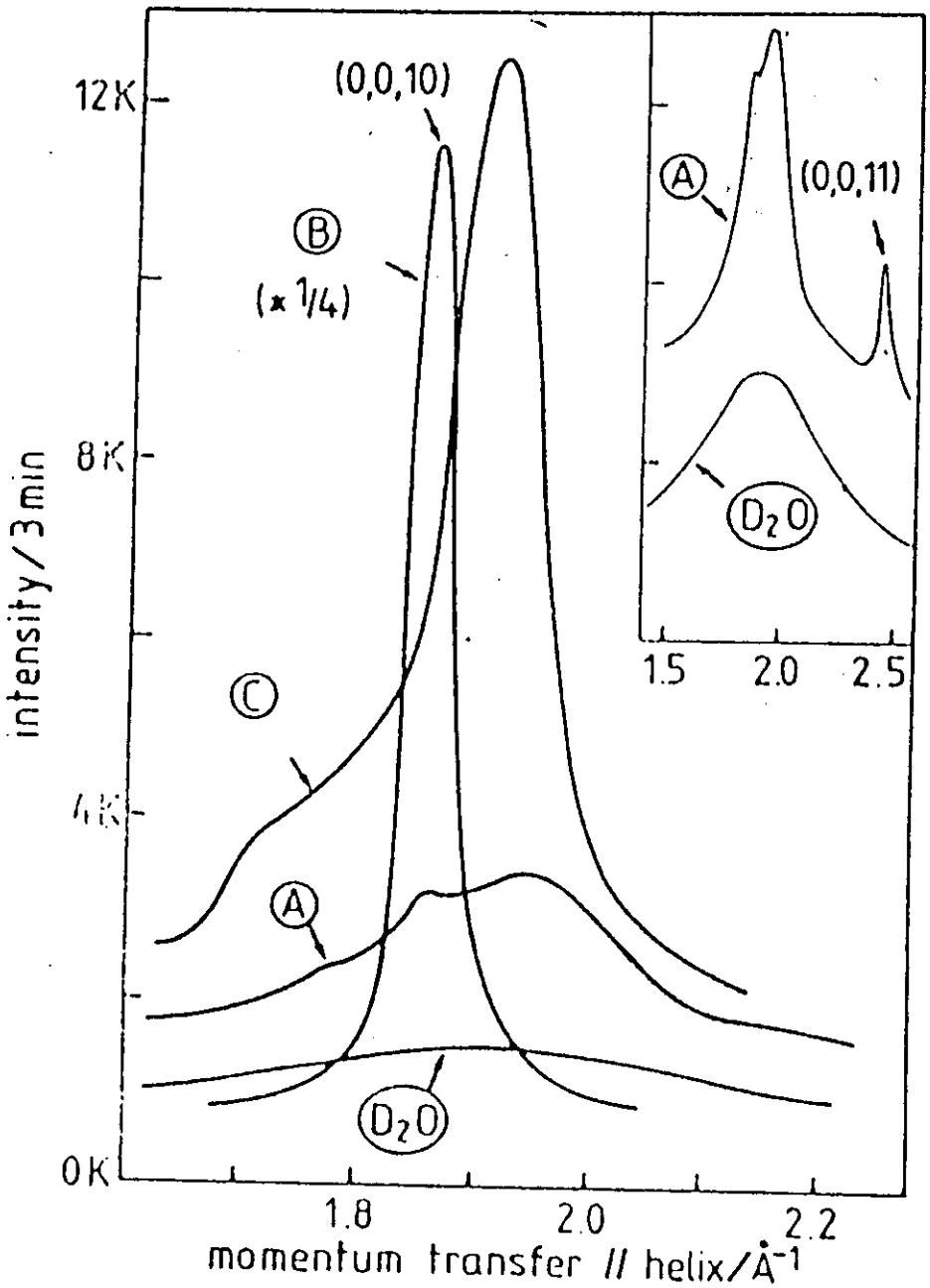

Elastic scans (within energy resolution of 0.23-THz FWHM) along the helix axis in the region of the first peak in the structure factor of water ($\simeq 1.92$ Å^{-1}; see curve for bulk D_2O). The results are given as lines because of the good statistics. The intensities are directly comparable since sample volume and experimental conditions were similar for all four scans. The symbols A, B, C correspond to the conformations of DNA (hydrated to 75% relative humidity by D_2O).

Grimm et al.

PRL 59 (1987) 1780.

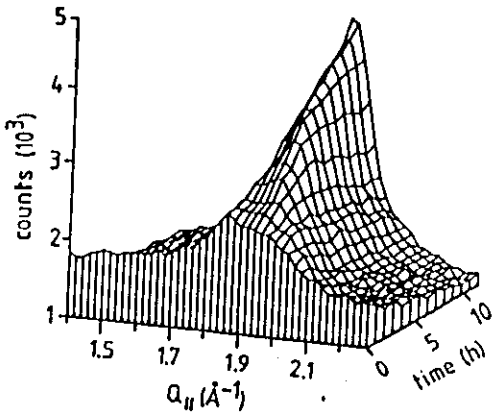

Fig. 2. Uncalibrated humitity variation of the scan through the WP. The A-sample was vacuum dried for five hours and then exposed to D_2O-humidified air (≈90% r.h.) during the measurement. The time scale refers to elapsed time after the first scan. Optimum A-DNA reflections were obtained for $1 \leq$ time/hour ≤ 5.

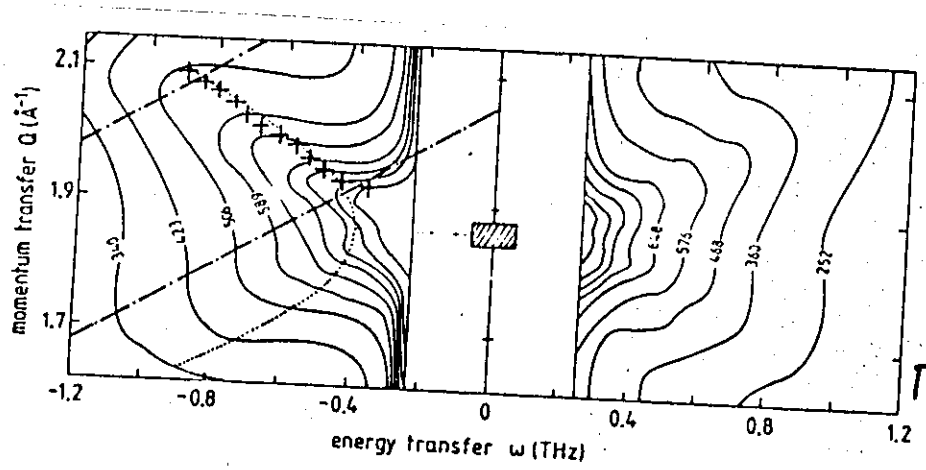

$\omega^2 = \omega_0^2 + v^2(\Delta Q)^2$

$v = 1.85 \pm 0.05 \frac{k}{s}$

$\Gamma = 0.12 \pm 0.01$ Å^{-1}

FIG. 2. Contour map of the scattered intensity from B-DNA in the $(Q_{\parallel},\omega)$ plane. The figures at the equidistant contour lines denote counts per about two minutes. Position and width of the peak shown in Fig. 1 is indicated by the shaded area. The dash-dotted lines correspond to the paths of the first and last scans displayed in Fig. 3. The crosses mark the fitted peak positions of those and similar scans. The apparent deviation of the cross for the lowest frequency is very likely due to the fact that the resolution ellipsoid "picks up" already some intensity from the (1,0,10) reflection. The dotted line corresponds to Eq. (3).

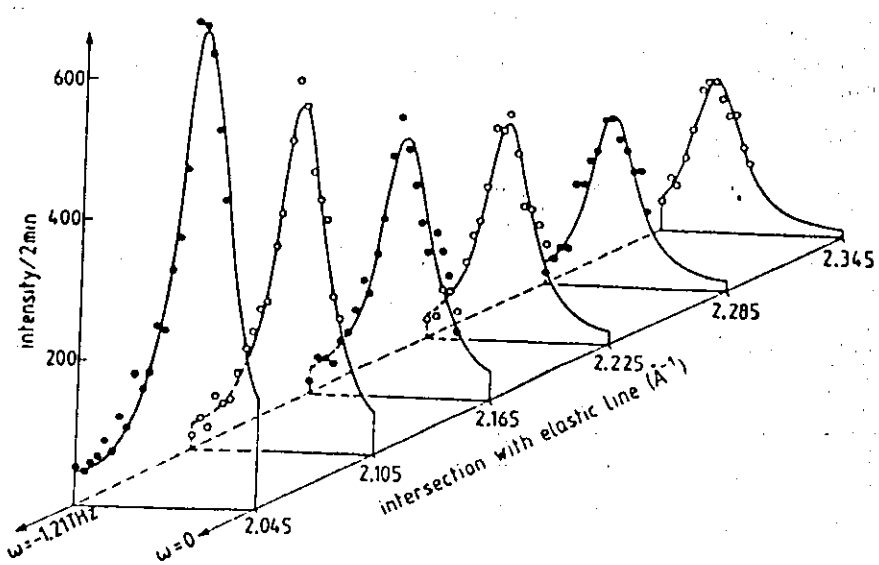

FIG. 3. Series of constant-velocity scans for B-DNA in the $(Q_{\parallel},\omega)$ plane as indicated in Fig. 2. The chosen velocity for the scan direction is 2.026 km/sec or 3.224 THz/Å^{-1}. The scans intersect the elastic line at the indicated values for $Q_{\parallel}$. The intensities correspond to the difference between the orientation of the momentum transfer parallel and perpendicular to the helix axis. The solid lines represent individual Lorentzians folded with the resolution of the spectrometer.

M.-C. Bellisent-Funel et al. Biophys. J. 56, 713 (1989)

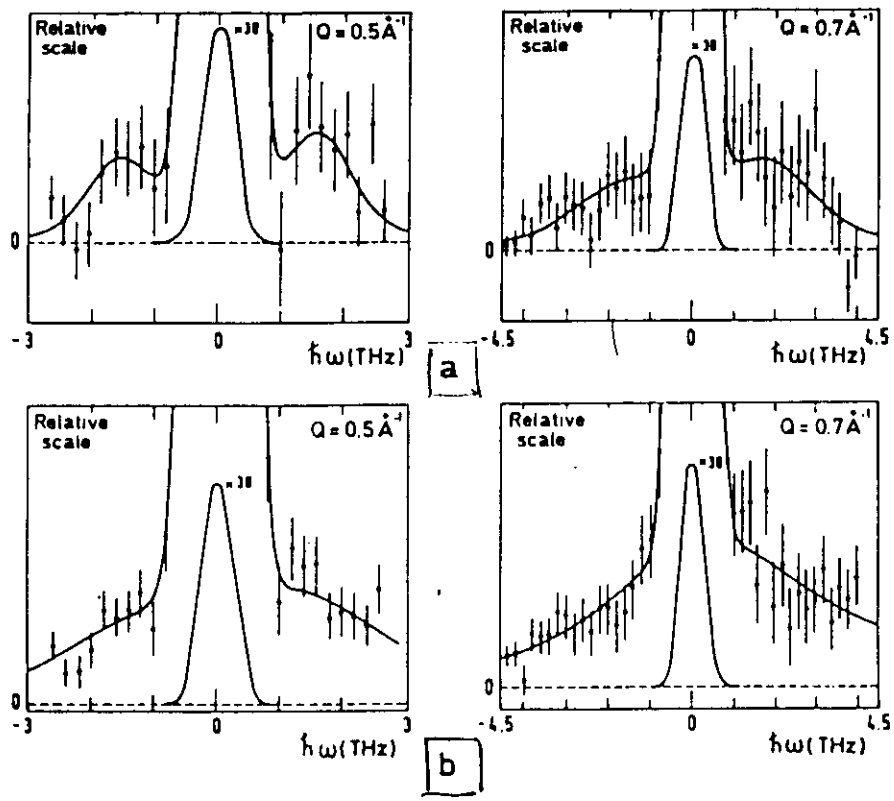

FIGURE 1 Scattered intensity I vs. $\hbar\omega$ from constant-Q scans at Q = 0.5 Å^{-1} and Q = 0.7 Å^{-1} for (*a*) dry phycocyanin, (*b*) D_2O-hydrated phycocyanin. Full curves represent least-square fits according to a damped harmonic-oscillator model (compare reference Teixeira et al., 1985 for details). The typical χ^2 values were ~1.3

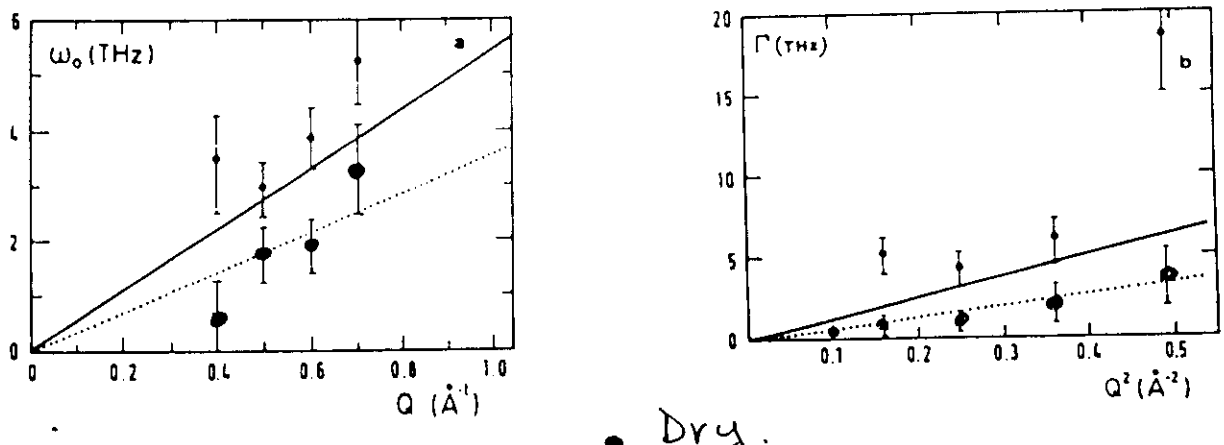

FIGURE 2 (*a*) Representation of the dispersion curve. (*b*) Linewidth, Γ, plotted against Q^2. (*Full line*) pure D_2O (Teixeira et al., 1985). (*Crosses*) dry *C*-phycocyanin. The dotted line (*a*) gives a velocity equal to 2,260 m.s.$^{-1}$. (*Full dots*) D_2O-hydrated *c*-phycocyanin.

Inelastic and quasi-elastic Neutron Scattering.

$S_{inc}(Q,\omega)$ { - Diffusion coefficients
- rotational / translational correlation times
- EISF
- vibrational density of states

$S_{coh}(Q,\omega)$ { - phonons
- brillouin scattering.

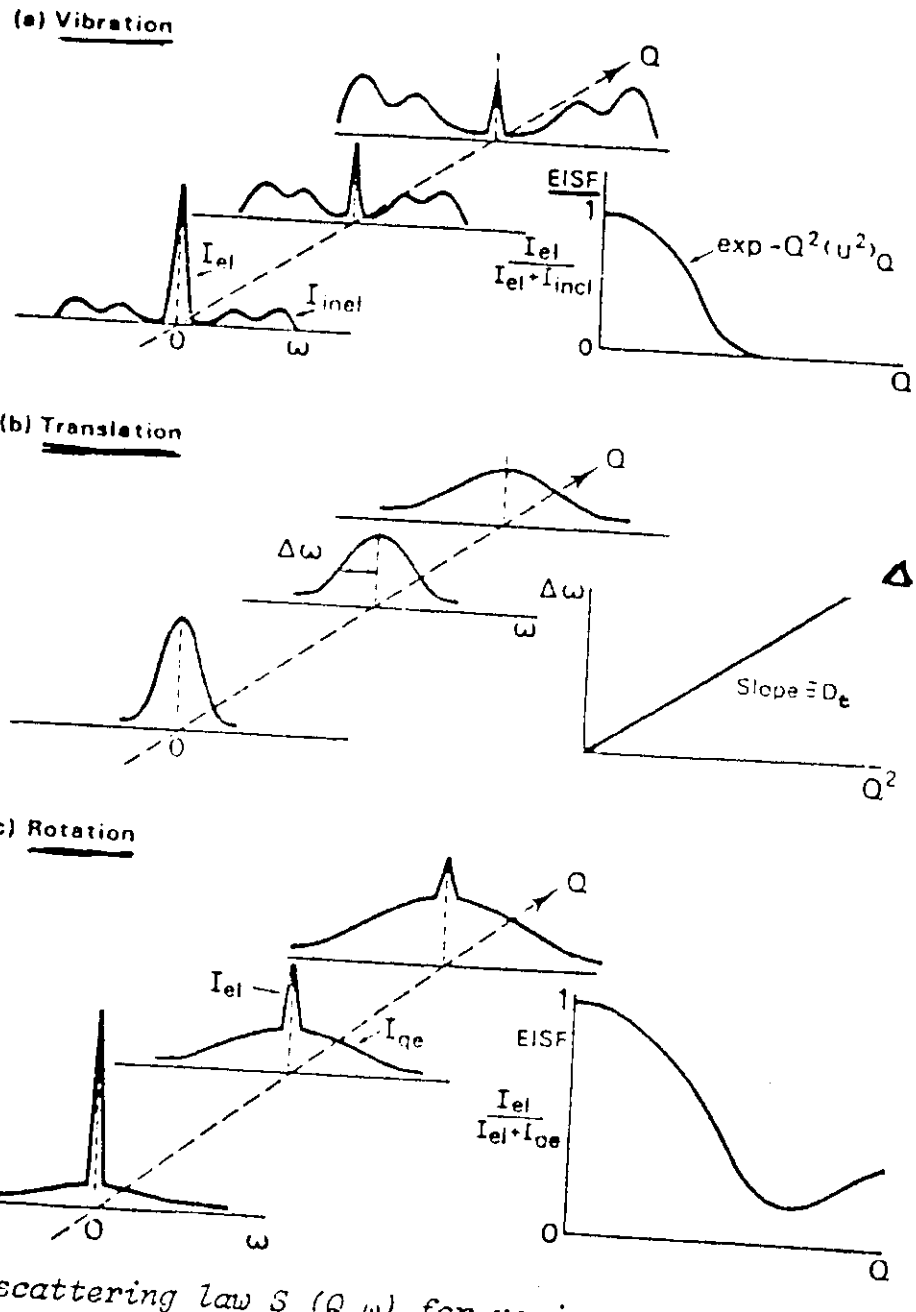

Incoherent scattering law $S_s(Q,\omega)$ for various motions.

Multi-state equilibrium

$$I_0 \overset{K_1}{\rightleftharpoons} I_1 \overset{K_2}{\rightleftharpoons} I_2 \cdots I_{n-1} \overset{K_n}{\rightleftharpoons} I_n$$

Taking I_0 as the reference state, we can define the statistical weight, ω_i, of a given state, I_i, as

$$\omega_i = \frac{[I_i]}{[I_0]} = K_i = \exp(-\Delta G_i/RT)$$

The partition function can be defined as

$$Q = \sum_{i=0}^{n} \omega_i = \sum_{i=0}^{n} \exp(-\Delta G_i/RT) = 1 + \sum_{i=1}^{n} \exp(-\Delta G_i/RT)$$

$$x_i = \frac{\omega_i}{Q} = \frac{\exp(-\Delta G_i/RT)}{Q}$$

$$\langle \Delta H \rangle = \sum^{n} x_i \cdot \Delta H_i = \frac{\sum \Delta H_i \cdot \exp(-\Delta G_i/RT)}{Q}$$

$$C_p^{ex} = \frac{\partial \langle \Delta H \rangle}{\partial T} = \left(\langle \Delta H^2 \rangle - \langle \Delta H \rangle^2 \right) / RT^2 + \langle \Delta C_p \rangle$$

It can be easily shown that

$$\frac{d \ln Q}{dT} = \frac{\sum \exp(-\Delta G_i/RT) \cdot \frac{\Delta H_i}{RT^2}}{Q} = \frac{\langle \Delta H \rangle}{RT^2}$$

$$Q(T) = \exp \int_{T_0}^{T} \frac{\langle \Delta H \rangle}{RT^2} dT$$

Biopolymers (1978) 17, 463-479

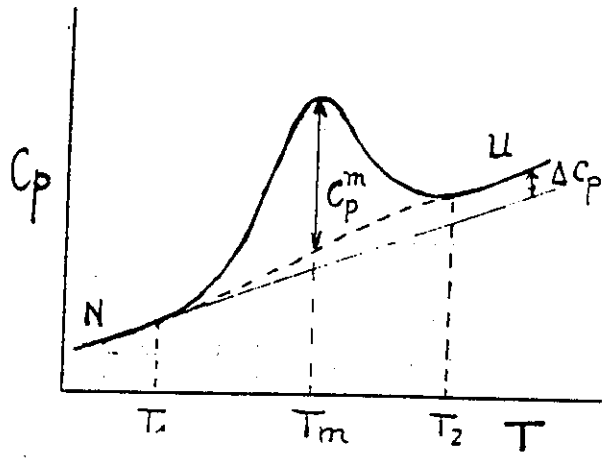

$$\Delta H = \int_{T_1}^{T_2} C_p \, dT$$

$$\Delta H^{v\text{-}H} = 4 R T_m^2 \frac{C_p^m}{\Delta H}$$

$\Delta H = \Delta H^{v\text{-}H} \Rightarrow$ Two-state

$\Delta H > \Delta H^{v\text{-}H} \Rightarrow$ *Intermediate states (multidomain proteins)*

$\Delta H < \Delta H^{v\text{-}H} \Rightarrow$ *Intermolecular co-operativity (associations)*

DSC $\rightarrow \Delta H,\ T_m,\ \Delta C_p \rightarrow \Delta H(T),\ \Delta S(T),\ \Delta G(T)$

- $\Delta H(T) = \Delta H(T_m) - \Delta C_p (T_m - T)$; $\Delta C_p = C_p(U) - C_p(N) = \text{constant}$
- $\Delta S(T) = \Delta S(T_m) - \Delta C_p \ln \frac{T_m}{T} = \frac{\Delta H(T_m)}{T_m} - \Delta C_p \ln \frac{T_m}{T}$

$$T = T_m \Rightarrow \Delta G(T_m) = 0 \Rightarrow \Delta S(T_m) = \frac{\Delta H(T_m)}{T_m}$$

- $\Delta G(T) = \Delta H(T) - T \cdot \Delta S(T) = \Delta H(T_m) \frac{T_m - T}{T_m} - \Delta C_p (T_m - T) + \Delta C_p T \ln \frac{T_m}{T}$

Two-state equilibrium model

$$N \overset{K}{\rightleftharpoons} D \quad ; \quad K = \frac{[D]}{[N]} \quad ; \quad x_D = \frac{[D]}{[N]+[D]} = \frac{K}{1+K}$$

Taking the N state as the reference state:

$$\langle \Delta H \rangle = \int_{T_0}^{T} C_p^{ex} dT = \Delta H \cdot x_D = \frac{K}{1+K} \Delta H$$

$$C_p^{ex} = \frac{\partial \langle \Delta H \rangle}{\partial T} = \Delta H \frac{\partial K / \partial T}{(1+K)^2} + x_D \frac{\partial \Delta H}{\partial T} = \frac{K}{(1+K)^2} \frac{\Delta H^2}{RT^2} + \Delta C_p \frac{K}{1+K}$$

$$T = T_m \Rightarrow x_D = x_N = 1/2 \Rightarrow K = 1 \Rightarrow \Delta G(T_m) = 0 \Rightarrow \Delta S(T_m) = \frac{\Delta H(T_m)}{T_m}$$

Then:

$$\Delta H(T) = \Delta H(T_m) + \int_{T_m}^{T} \Delta C_p \, dT$$

$$\Delta S(T) = \frac{\Delta H(T_m)}{T_m} + \int_{T_m}^{T} \Delta C_p \frac{dT}{T}$$

$$\Delta G(T) = \Delta H(T) - T \cdot \Delta S(T)$$

$$T = T_m \Rightarrow \Delta H^{v.H} = 4 R T_m^2 \frac{C_p^m}{\Delta H}$$

DSC scans:

For the buffer (solvent): $C_{p,b} = m_b \cdot c_{p,b}$

For the protein solution: $C_{p,p} = m_p \cdot c^{\circ}_{p,p} + m'_b \cdot c^{\circ}_{p,b}$

where

m_b = mass of solvent in the cell

$c^{\circ}_{p,b}$ = specific heat capacity of the buffer solution

$c^{\circ}_{p,p}$ = specific heat capacity of the protein

m_p = mass of protein in the calorimetric cell

m'_b = mass of solvent in the sample cell

$$C_{p,p}^{\circ} = [C_{p,p} - C_{p,b} + (m_b - m'_b) c^{\circ}_{p,b}] / m_p$$

Since $m_b - m'_b$ = mass of solvent displaced by the protein,

$$(m_b - m'_b) V_b^{\circ} = m_p \cdot V_p^{\circ}$$

where V_p° and V_b° are the partial specific volumes of the protein and solvent respectively

Therefore

$$\underline{\underline{c^{\circ}_{p,p} = (C_{p,p} - C_{p,b}) / m_p + c^{\circ}_{p,b} (V_p^{\circ} / V_b^{\circ})}}$$

$$c^{\circ}_{p,p} \times M = \underline{\underline{C_p}} \text{ (molar heat capacity)}$$